8-7-2010

Tissue engineering cartilage for focal defects

Scott Chi Tran

TISSUE ENGINEERING CARTILAGE FOR FOCAL DEFECTS

By

Scott Chi Tran

A Thesis
Submitted to the Faculty of
Mississippi State University
in Partial Fulfillment of the Requirements
for the Degree of Master of Science
in Biomedical Engineering
in the Department of Agricultural and Biological Engineering

Mississippi State, Mississippi

August 2010

TISSUE ENGINEERING CARTILAGE FOR FOCAL DEFECTS

By

Scott Chi Tran

Approved:

Steve Elder Associate Professor of Agricultural and Biological Engineering Major Professor	Jun Liao Assistant Professor of Agricultural and Biological Engineering Committee Member
Lakeisha Williams Assistant Professor of Agricultural and Biological Engineering Committee Member	James Cooley Associate Professor of Pathobiology and Population Medicine of the College of Veterinary Medicine Committee Member
Steve Elder Associate Professor of Agricultural and Biological Engineering Graduate Coordinator	Sara Rajala Dean of the Bagley College of Engineering

Name: Scott Chi Tran

Date of Degree: August 7, 2010

Institution: Mississippi State University

Major Field: Biomedical Engineering

Major Professor: Steve Elder

Title of Study: TISSUE ENGINEERING CARTILAGE FOR FOCAL DEFECTS

Pages in Study: 93

Candidate for Degree of Master of Science

Articular cartilage provides a near frictionless surface for the articulating ends of bones. Cartilage functions to lubricate and transmit compressive forces resulting from joint loading and impact. If damaged, whether by traumatic injury or disease, cartilage lacks the ability for self-repair.

This study explores the production of scaffold-free cartilage and investigates the effect of Tissue Growth Technologies' CartiGen Bioreactor on the cartilage. Chondrocyte and bone marrow-derived stem cell (BMSC) attachment to chitosan is also investigated in hopes of producing a bilayered construct for osteochondral repair.

Results demonstrate that culturing of scaffold-free cartilage in the CartiGen bioreactor resulted in an enhancement of the scaffold-free cartilage's biomechanical and biochemical properties and that the chitosan microspheres were able to successfully support porcine chondrocyte and BMSC attachment. Results from both studies are encouraging for future work involving tissue engineered cartilage.

DEDICATION

This work is dedicated to my parents, Chan and Tammy, and my brother Long. My family has provided me with every opportunity that I could ever ask for and this work would not have been possible without their support and love. Thank you for everything that you have done.

ACKNOWLEDGEMENTS

I would like to acknowledge and thank everyone who has been involved with my research and studies these past two years. First, I would like to thank my major professor, Dr. Steve Elder, for his help and guidance with my research. Many thanks to the members of my thesis committee, Dr. Jun Liao, Dr. Lakiesha Williams, and Dr. Jim Cooley for their time, input, and feedback. Finally, I want to thank Joe Chen, John Clemmer, and Lauren Priddy for their time, support, and friendship. It has been a great pleasure to learn and grow with all of you during our time at Mississippi State.

TABLE OF CONTENTS

Page

LIST OF FIGURES

FIGURE Page

LIST OF ACRONYMS

OA = Osteoarthritis

ECM = Extracellular Matrix

GAG = Glycosaminoglycans

TKA = Total Knee Arthroplasty

UKA = Unicompartmental Knee Arthroplasty

ACI = Autologous Chondrocyte Implantation

TE = Tissue Engineering

TGF-β = Transforming Growth Factor - Beta

CDMP = Cartilage Derived Morphogenic Protein

FGF = Fibroblast Growth Factor

IGF = Insulin-like Growth Factor

DMEM = Dulbecco's Modified Eagle Medium

FBS = Fetal Bovine Serum

PBS = Phosphaste Buffered Saline

DD =Degree of Deacetylation

HA = Hydroxyapatite

BMSC = Bone Marrow-Derived Mesenchymal Stem Cell

HMDS = Hexamethyldisilazane

CaP = Calcium Phosphate

CHAPTER I

INTRODUCTION

Articular Cartilage

Articular cartilage, also known as hyaline cartilage, is a smooth and glossy tissue that lines the ends of articulating bones. Cartilage possesses a high capacity to bear load and a low coefficient of friction, promoting the smooth articulation of one bone against another. Articular cartilage serves as a shock absorber and functions to transmit compressive forces resulting from joint loading and impact. Damage to cartilage can be caused by trauma, disease, or normal wear and tear and can lead to irritation, pain, and reduced joint mobility. Cartilage lacks a direct blood supply, and thus has a limited capacity for self repair. If left untreated, further degradation may occur, causing damage to the surrounding healthy cartilage. These lesions or defects in cartilage may progress towards osteoarthritis (OA). At this time, a satisfactory and long-term solution has yet to be identified for healing damaged cartilage. Advances in knowledge and technology have led tissue engineering to emerge as a promising therapy for generating a functional tissue substitute with properties similar to native tissue. In order to achieve this goal, a basic understanding of the composition, structure, and behavior of cartilage is required.

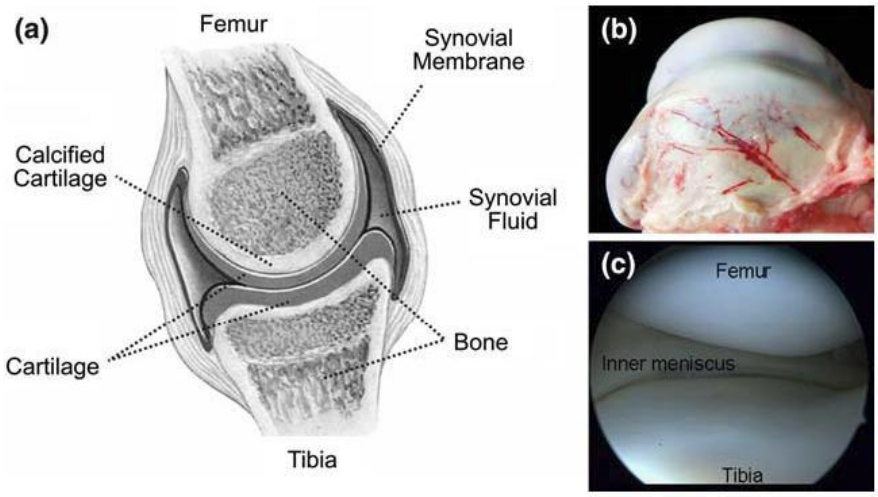

Figure 1.1 Sketch of the knee joint (a), *side view* on femoral condyle of an open joint (b), and *arthroscopic view* of a healthy human knee joint (c). From [1].

Composition

Articular cartilage is composed of cells known as chondrocytes, which are surrounded by a complex extracellular matrix (ECM). Chondrocytes only account for about 1% of the volume of articular cartilage with the other 99% represented by ECM. Articular cartilage consists of mostly water, which accounts for about 70-80% of the tissue's weight. The remaining solid fraction of the tissue is composed primarily of collagen (10-30%) and proteoglycans (3-10%). The organization of the collagen and proteoglycans provides articular cartilage with its unique viscoelastic property.

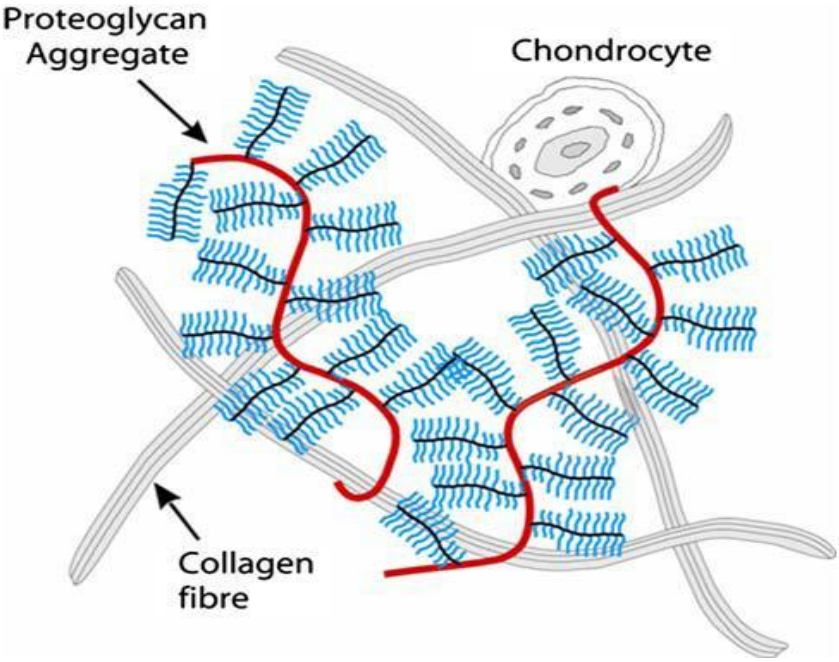

Figure 1.2 Illustration of the extracellular matrix (ECM) composition of articular cartilage. From [1].

Chondrocytes are the highly specialized cells of articular cartilage and are sparsely spread throughout the tissue. As a result, articular cartilage has the lowest volumetric cellular density of any tissue in the human body [1]. Chondrocytes are spheroidal shaped cells that exhibit no cell-to-cell contact and often reside as single, isolated cells in small cavities known as lacunae. Chondrocytes play an essential role in the maintenance of the tissue by synthesizing all the necessary components of the ECM. Matrix metabolism is therefore regulated by chondrocytes, as the cells control the secretion and degradation of ECM proteins. Although the overall metabolic activity of cartilage is very low due to the low population of cells within the tissue, the individual metabolic activity of chondrocytes is very high. Microscopically, chondrocytes possess a prominent Golgi Apparatus and a large, granular endoplasmic reticulum, both of which

help to support the cell's high metabolic activity. Because articular cartilage is avascular, nutrient and oxygen transport to chondrocytes is facilitated by diffusion from the synovial fluid into the cartilage matrix and thus is a very slow process. Chondrocytes demonstrate the distinct ability to sense changes in the surrounding mechanical environment, and are known to modify matrix production in response to mechanical stimuli.

Collagen is a structural protein that makes up about two-thirds of the dry weight of articular cartilage. Collagen is composed of repeating chains of amino acids which form into a characteristic triple helix structure. Type II collagen is the most abundant form found in articular cartilage, although types III, VI, IX, X, XI, XII, and XIV are also present in much smaller amounts. The tensile strength of articular cartilage is provided by the abundance of type II collagen, but is also dependent on the amount of cross-linking of collagen and the zonal changes in fiber organization. Collagen turnover is a very slow process, with collagen generally lasting an entire lifetime.

Proteoglycans are macromolecules composed of a core protein to which numerous negatively charged glycosaminoglycans (GAG) subunits are attached. The two main types of GAGs are chondroitin sulfate and keratin sulfate. Proteoglycans can exist as monomers or can aggregate and bind to a hyaluronic acid chain via link proteins to form large proteoglycan aggegrates. The large size of these proteoglycan aggregates, or aggrecans, keeps the proteoglycans restrained within the collagen network. The entrapment of proteoglycans, along with the negative charge of the numerous GAG side chains, provides the compressive stiffness of articular cartilage.

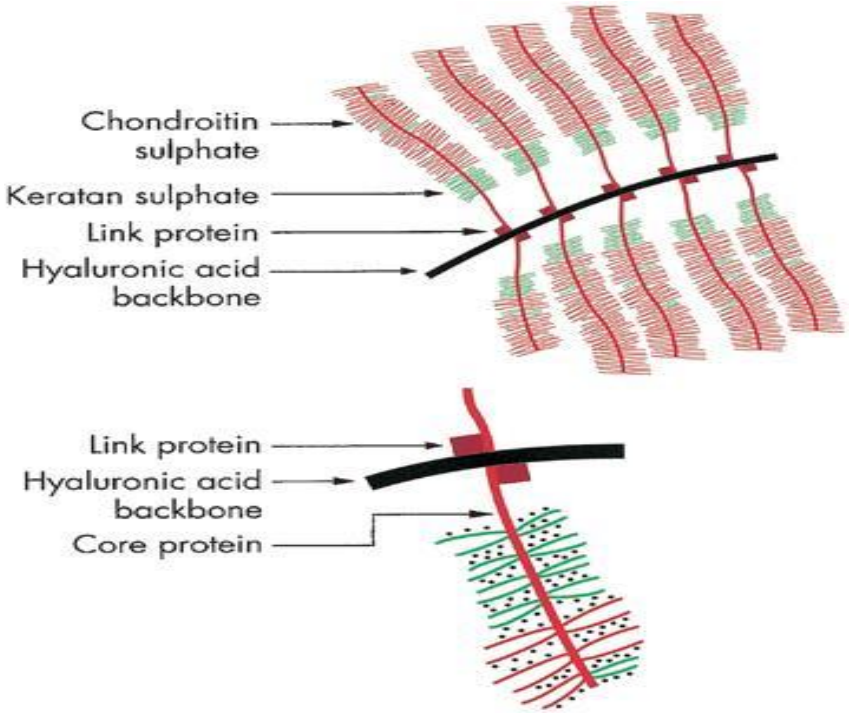

Figure 1.3 Schematic representation of the molecular organization of an aggregated proteoglycan molecule. From (bjr.birjournals.org)

Structure

Articular cartilage is comprised of four distinct zones spanning from the articular surface down to the subchondral bone. The four zones are known as superficial (or tangential), middle (or transitional), deep (or radial), and the calcified cartilage zone. These four zones can be identified by differences in biochemical content and organization, as well as chondrocyte number, shape, and metabolic activity.

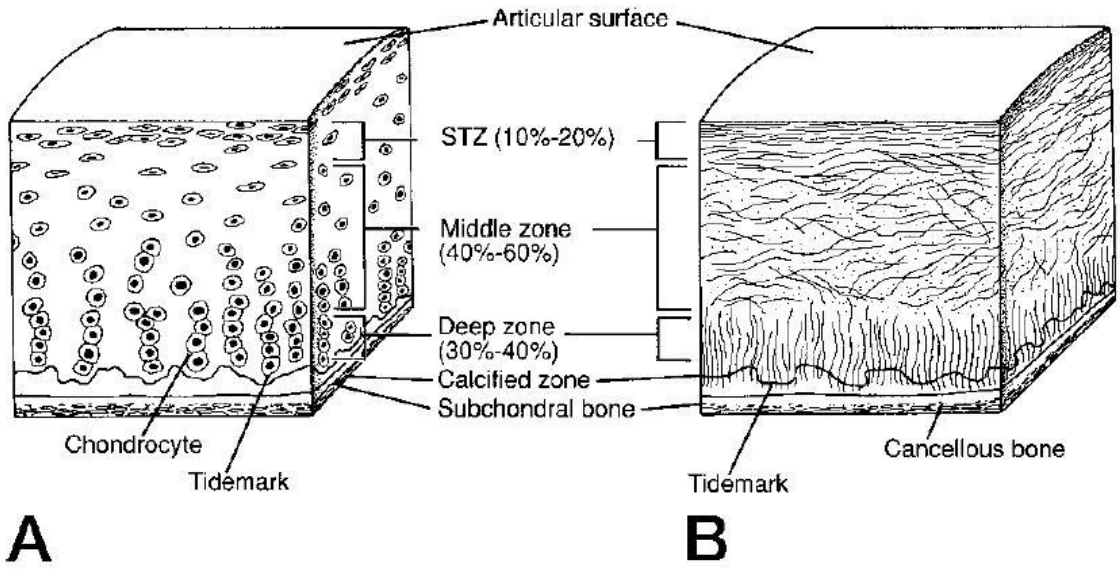

Figure 1.4 Structure of articular cartilage. (**A**) Schematic diagram of the cellular organization throughout the zone of articular cartilage. (**B**) Diagram of collagen fiber architecture. From [2].

The superficial, or tangential, zone is the thinnest of all the layers and forms the gliding surface of joints. This zone is composed of small diameter collagen fibers that are densely packed and arranged parallel to the joint surface. The tangentially organized collagen fibers provide the superficial zone the tensile and shear strength necessary to withstand forces encountered on the joint surface. High collagen content, in addition to low proteoglycan content and low permeability, makes the superficial zone the highest water content zone. Chondrocytes of this region exhibit flattened, elongated shapes and are also oriented parallel to the joint surface. These cells are coated by a thin layer of lubricin that helps to provide a smooth gliding surface for joints and prevents wear and tear from frictional forces.

The middle, or transitional, zone is thicker than the superficial zone making up about 60% of the tissue's total thickness. The middle zone is composed of larger

diameter collagen fibers with a mesh-like, random orientation. Cell density in the middle zone is lower than the superficial zone, and chondrocytes in the middle zone take on a more spherical shape with orientations perpendicular to the joint surface. Proteoglycan content is highest in this zone and in conjunction with the abundant ECM, makes the middle zone ideal for withstanding compression.

The deep, or radial, zone is the last region of purely hyaline-tissue before reaching bone. Collagen fibers in this zone form bundles aligned parallel to one another, but oriented perpendicular to the joint surface. The cells of the deep zone become more spheroidal in shape and begin to organize into columns orientated perpendicular to the joint surface.

A fine borderline known as the "tidemark" separates the deep zone from the calcified cartilage zone. The zone of calcified cartilage serves as a transitional zone between the articular cartilage and the subchondral bone. Long collagen fibers from the deep zone extend into the calcified zone and ultimately anchor into the subchondral bone, providing fixation between the two tissues.

The ECM exhibits zonal organization as well as matrix organization dependent on the distance from the chondrocyte cell membrane. These regions differ not only in distance from the cells, but also in regard to biochemical composition and organization. The region immediately surrounding the chondrocyte is the pericellular matrix, and is characterized by fine collagen fibers and an abundance of proteoglycans. The territorial matrix surrounds the cells and the pericellular matrix and provides protection from mechanical impacts by surrounding the chondrocytes in a mesh of fine collagen fibers. The region furthest away from the cell is termed the interterritorial matrix and comprises the majority of articular cartilage. The proteoglycan content and collagen organization of

the interterritorial matrix are dependent on the distance from the joint surface, and coincide with the zonal organization discussed previously.

Function

The primary function of articular cartilage is to provide a load bearing surface with low friction and minimal wear. Articular cartilage allows for the transmission of large loads between bones, while simultaneously allowing the smooth articulation between the two bones. The ability of articular cartilage to withstand high cyclic and intermittent loads over several decades with no signs of degeneration is a result of the tissue's unique biochemical and mechanical characteristics.

Since cartilage is essentially a porous, fluid-saturated matrix, it can be viewed as a biphasic medium. The fluid phase is comprised of water and electrolytes, while ECM components such as collagen and proteoglycans constitute the solid phase. Articular cartilage can be characterized as a nonlinear, viscoelastic, anisotropic material. In solution, the negatively charged GAG chains of proteoglycans repel one another, causing the aggrecan to distend and occupy a large volume. In the cartilage matrix, the aggrecan is entangled within the collagen matrix, limiting the dispersion of the aggrecan. Compression reduces spacing and increases the repulsive forces between the negatively charged sites, adding to the compressive stiffness of the cartilage. The mechanical properties of articular cartilage are highly dependent on the fluid flow through the tissue. Initial loading results in an immediate increase in interstitial pressure, causing fluid to flow out of the ECM, and when the load is removed, fluid flows back into the tissue. As fluid flows through the tissue, high drag forces are created due to articular cartilage's low permeability. This prevents fluid from quickly escaping the matrix, allowing the fluid

phase to support the majority of the load instead of the solid matrix. After a prolonged period of loading, pressurization drops, fluid is no longer exuded from the tissue, and the tissue reaches equilibrium. During this process, more and more of the force is transferred to the solid fraction of the tissue until equilibrium is reached, at which point the solid fraction supports the entire load. Certainly, the response of articular cartilage to load can be attributed to the structure-function relationship between its components, but more importantly relies on the interdependence between the tissue's fluid flow and matrix deformation.

Articular Cartilage Damage

Traumatic injury, repetitive loading, joint misalignment, and degenerative joint disease can all damage articular cartilage, resulting in the reduced or complete loss of tissue function. Unfortunately, once damaged, the natural healing response of articular cartilage is unable to restore a fully functional tissue. Damage to articular cartilage can be classified as either a chondral or an osteochondral defect. Chondral defects are those that do not penetrate to the subchondral bone, whereas osteochondral defects penetrate the subchondral bone, thereby gaining access to the bone's vasculature.

In general, the body's natural healing response involves three phases: necrosis, inflammation, and repair [3]. Necrosis begins immediately after injury occurs and involves cell death due to trauma. The inflammatory phase follows necrosis and is fully dependent on the vascular system. Increased blood flow and vasodilatation results in the formation of a dense fibrin network rich in inflammatory cells. The repair phase is characterized by the creation of vascular granulation tissue and in some instances the

formation of a scar. During the repair phase, the long process of remodeling begins in order to restore identical tissue.

Chondral, or partial-thickness defects, are unable to heal spontaneously. Due to the lack of vascularization within articular cartilage, the inflammatory and repair phases of the healing response are unable to occur. Without a vascular system, phagocytic cells, pluripotent cells, and growth factors are unable to be delivered to the area of trauma. In addition, surrounding chondrocytes are unable to migrate to the injury site due to being entrapped within the ECM. The collagen network at the site of injury becomes disrupted, resulting in GAG release, and thus weakening the tissue. Since no significant healing takes place, these defects can result in osteochondral defects.

Osteochonral defects penetrate into the vasculature of subchonral bone and elicit the more characteristic repair response. The repair process of full-thickness defects has been extensively described by Shapiro et al. [4]. Disruption of the vasculature causes blood to fill the defect, trapping red blood cells, white blood cells, and stem cells from the marrow. The blood clot initially becomes a highly vascularized scar-like tissue, but soon transforms into a fibrous cartilage-like tissue. Poor integration occurs between the inferior fibrocartilage and the surrounding native tissue and areas of discontinuity are frequently observed. The repair tissue lacks sufficient mechanical properties, becomes fibrillated and begins to degenerate. The tissue's poor functionality affects the biomechanics of native tissue and alters the loading environment of the joint. Ultimately, lesions that are left untreated will become progressively worse and lead to osteoarthritis.

Osteoarthritis

Osteoarthritis (OA) is the most common type of arthritis and is characterized by the degeneration and eventual loss of cartilage in diarthroidal joints. Diagnosis of OA is made radiographically and clinically. Radiographically, the loss of articular cartilage is accompanied by changes in the underlying bone including development of marginal outgrowths, osetophytes, and increased thinness of the bony envelop (bony sclerosis) [5]. Clinical symptoms are usually manifested in joint pain and reduced function. OA can affect any diarthroidal joint, but is most commonly seen in the hands, hips, and knees. Based on the severity, OA is graded on a scale from 1 to 4. In Grade 1 OA, the joint space is preserved and OA is considered mild. Grade 4 is considered severe OA and is characterized by the complete loss of articular cartilage resulting in bone-on-bone articulation. OA is one of the leading disabilities of the developed countries and is estimated to affect about 27 million people in the United States [6]. The prevalence of OA increases with age and as the population ages, the socio-economic burden of OA will become even greater [7].

Current Therapies

In order to repair damaged cartilage, the inherent deficiencies found in articular cartilage must be overcome [8]. Most reparative methods have focused on introducing new cells capable of chondrogensis and accessing the subchondral blood supply. Although the natural repair response of articular cartilage results in the formation of inferior fibrocartilage, many surgical therapies are based on this repair mechanism to alleviate joint pain.

Debridement, Chondral Shaving, Lavage

Debridement and chondral shavings are procedures that are performed arthroscopically to remove areas of damaged cartilage. Lavage, or simply rinsing of the joint with a physiological fluid such as Ringers lactate, is usually carried out in conjunction with debridement in order to remove degradation products from the joint. These procedures do not repair or restore cartilage, but rather serve to temporarily relieve pain and irritation. Since debridement, chondral shaving, or lavage are unable to restore cartilage or alter disease progression, they are no longer recommended for treatment of osteoarthritic knees [9].

Abrasion Arthroplasty, Subchondral Drilling, Microfracture

Abrasion arthroplasty, subchondral drilling, and microfracture are all reparative strategies that are based on the penetration of subchondral bone in order to gain access to the vasculature of the bone. The defect is then filled with bone marrow containing pluripotent stem cells leading to blood clot formation and generation of fibrocartilage repair tissue [10]. Microfracture has replaced the outdated abrasion arthroplasty and subchondral drilling as the most popular one-stage arthroscopic procedure. Microfracture involves the removal of damaged cartilage, forming a well-defined defect. Microfractures are created using a specially bent awl which creates V-shaped perforation holes 2 mm in diameter and 3 mm apart. Bleeding from the bone marrow is induced and the blood clot adheres to the surface of the exposed bone, which begins the healing process. Microfracture yields the best long-term results in young, active patients with cartilage defects smaller than 2.5 cm^2 [11].

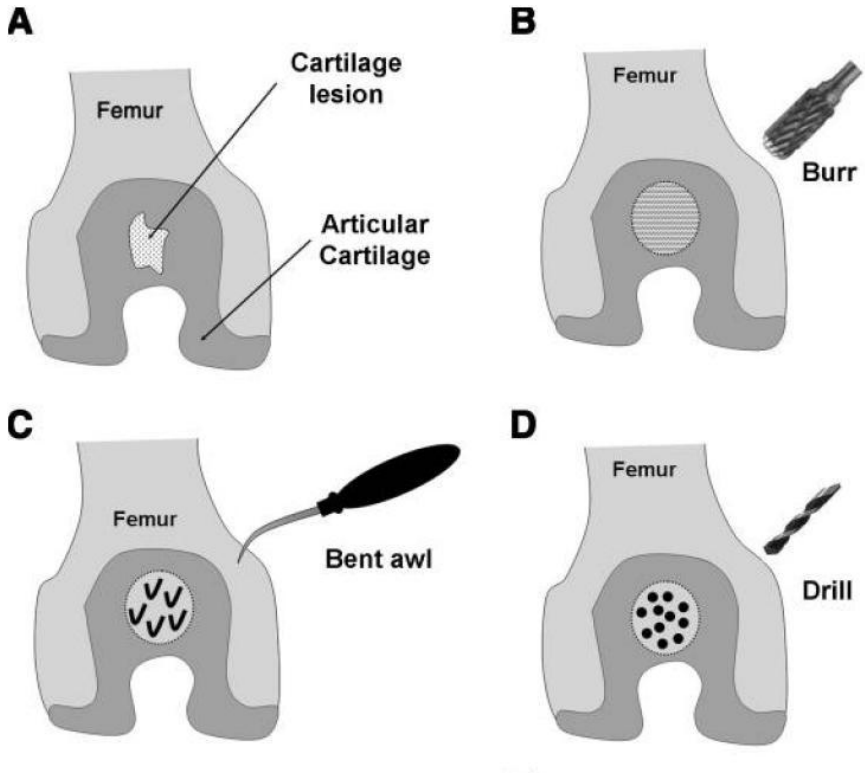

Figure 1.5 Different marrow stimulation techniques used for the treatment of cartilage lesions and the associated tool of operation. (A) Typical femoral cartilage lesion, (B) abrasion arthroplasty carried out by automated burr, (C) microfracture carried out by bent awl, (D) subchondral drilling carried out by automated driller. From [12].

Knee Replacement

When less invasive treatments are no longer an option, such as in end-stage OA, total knee arthroplasty (TKA) may be a patient's last option. Although TKAs do not alter the progression of OA, the procedure does reduce pain and improve function. Total knee replacements are performed if both the medial and lateral compartments must be replaced. If only the medial or lateral compartment must be replaced, then a unicompartmental knee arthroplasty (UKA) can be performed. Knee arthroplasty involves the resurfacing of tibial and condylar surfaces by removing enough bone for the placement of prosthetic components, which are commonly cemented to the bone [13].

Good fixation and restoration of the normal anatomical alignment are keys for a successful knee arthroplasty. The primary causes for failure or revisions of knee arthroplasties are aseptic loosening, instability, and mal-alignment [14]. TKAs have shown long-term success with some replacements lasting up to 20 years [15].

Tissue Grafts

The implantation of perichondrial and periosteal grafts has been explored as a possible repair technique for osteochondral defects. Since periosteum is easier to obtain and more abundant than perichondrium [16], periosteal grafts are more widely used. Carranza-Bencan et al. demonstrated that resurfacing defects using perichondrial and periosteal grafts produced superior results over the control group. The chondrogenic potential of periosteum is derived from the chondrocyte precursor cells in the cambial layer and has been demonstrated during fracture repair [17]. Implantation of periosteum requires the creation of a full-thickness defect and removal of subchondral bone. The tissue graft is then implanted into the defect with the cambial layer directed upward towards the articular cartilage and fixed in place with fibrin glue [16]. In addition to the periosteal chondrocyte precursor cells, mesenchymal stem cells from the marrow are also introduced since debridement of the subchondral bone occurs. Although good results have been reported with periosteal grafts, there is very limited clinical experience using this technique. Therefore, further studies must be conducted in order to determine the exact role of chondrocyte precursor cells in the repair response versus stem cells released from the subchondral bone.

Osteochondral Transfers

Osteochondral transfer is based on the transplantation of an entire osteochondral unit, which includes the intact cartilage tissue and its underlying bone. Both autologous and allogenic grafts have been widely used to repair medium and large osteochondral defects. Autologous osteochondral transplantation, or mosaicplasty, involves harvesting cylindrical osteochondral plugs from a non-weight bearing area of the joint for transplantation to the defect area. The osteochondral plugs for allogenic grafts are harvested from organ donors instead of taking plugs from the recipient's own joint. The plugs are press fitted into the defect site and the areas between the plugs are filled by fibrocartilage produced by the subchondral bone. Autologous grafts present no concerns regarding an immunological response; however, a limited supply of autogenous tissue and donor site morbidity are glaring issues. Furthermore, fitting the graft to match the topology of the surrounding joint is a difficult task. On the other hand, allogenic grafts can be harvested from the same location as the defective area, allowing for easy restoration of the joint's congruous surface. With allogenic grafts, donor age may vary so the grafts can be harvested from younger patients. The major disadvantages of allogenic grafts are the risks for an immune response and transmission of an infectious disease from the donor.

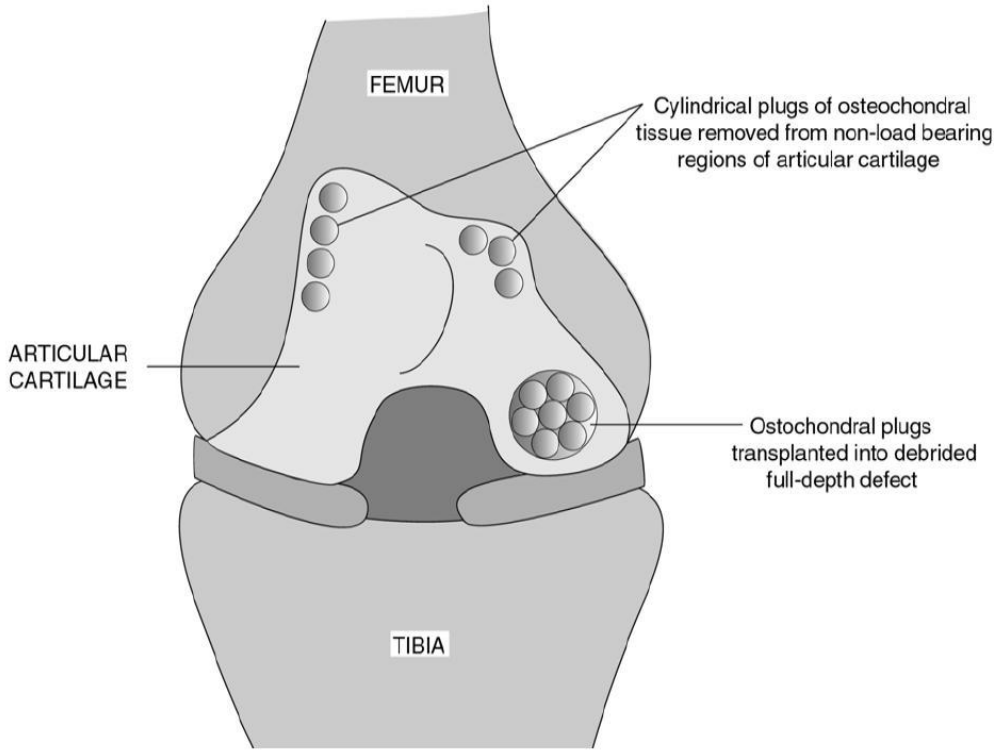

Figure 1.6 Schematic diagram illustrating steps involved in osteochondral transfer. From [18].

Autologous Chondrocyte Implantation (ACI)

Autologous chondrocyte implantation involves arthroscopically harvesting a healthy biopsy from a non-load bearing area of articular cartilage. The chondrocytes are then isolated by enzymatic digestion and expanded in culture. After the chondrocytes are expanded to a sufficient number, a second procedure is performed to debride the area and a periosteal flap taken from the upper tibial surface is sutured over the defect. The periosteal flap is sealed around the edges with fibrin glue and the autologous chondrocytes are injected underneath the flap into the defect site. Results from ACI have shown formation of hyaline-like repair tissue, as well as pain relief and restored joint function in 80-90% of patients [19]. Studies have shown good results following

treatment of osteochondral lesions, with durable results lasting up to 11 years [20]. However there are many disadvantages such as leakage of chondrocytes from the defect site, uneven distribution of chondrocytes, and periosteal hypertrophy [21]. Further investigation of the biochemical and mechanical nature the reparative tissue formed by this technique is necessary to assure ACI's superiority over existing treatments [8].

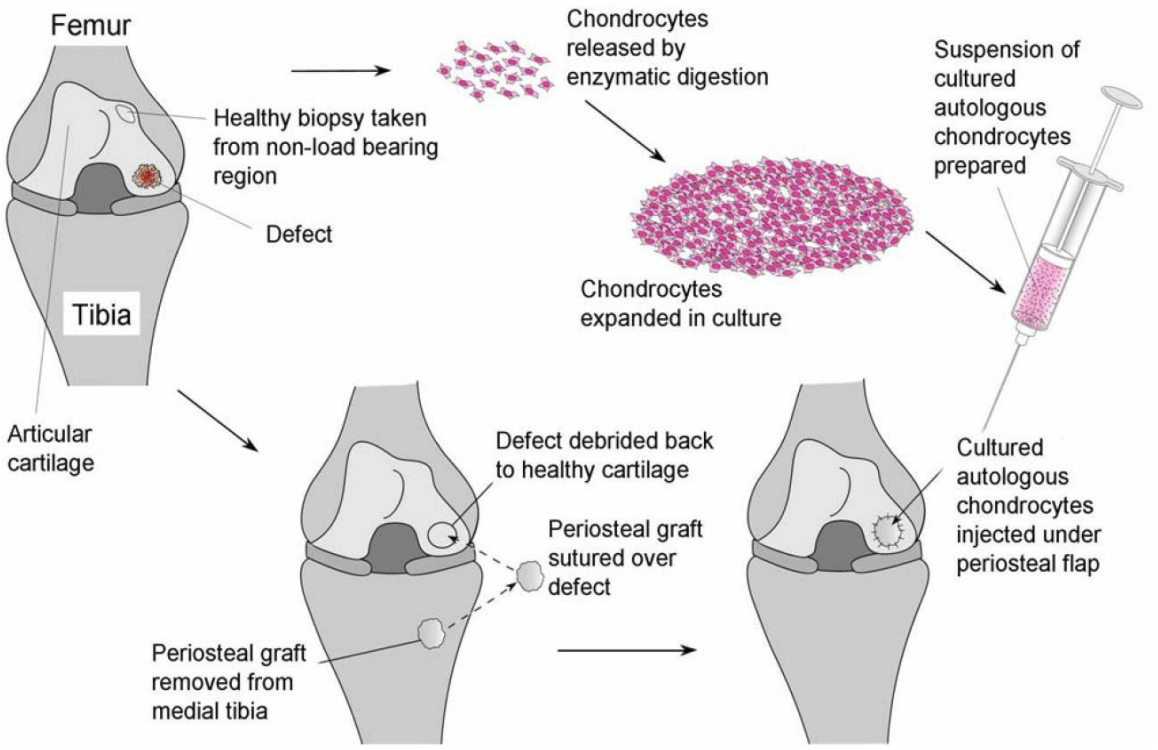

Figure 1.7 Schematic diagram showing the different stages involved in the process of autologous chondrocyte implantation. From [18].

Each of the aforementioned treatments has shown limited success in demonstrating long-term repair and all exhibit undesirable side effects. Most of the success has been seen in small lesions with fibrocartilage being observed as the primary repair tissue, which possesses inferior mechanical properties and often deteriorates over

time. Tissue engineering is an evolving field that may serve as an alternate approach for providing articular cartilage repair without the negative drawbacks of current therapies.

Tissue Engineering

Tissue engineering (TE) is a multidisciplinary field, which applies the principles of engineering and the life sciences to develop tissues aimed at restoring, maintaining, or improving tissue function [22]. Tissue engineering is comprised of the single use or combination of scaffolds, cells, and signaling molecules. The goal of articular cartilage tissue engineering is to generate tissue *in vitro* that is biochemically and mechanically identical to native articular cartilage for implantation *in vivo*. Much focus has been given to *in vitro* tissue engineering, because of the possibility of immediate functionality. The ability to manipulate nutrient supply, cell signals, and mechanical stimuli to ensure the tissue's biochemical and biomechanical functionality is necessary before implantation into the demanding environment of a joint.

Cell Source

Many cell sources have been investigated for tissue engineering articular cartilage including chondrocytes (articular, auricular, and costal) and mesenchymal stem cells (bone marrow and adipose). Chondrocytes seem to be the most logical choice since they are found in native cartilage, produce ECM, and are already differentiated into the desired phenotype. Although chondrocytes have been extensively used for cartilage repair, these cells present two major concerns: lack of donor tissue and instability during monolayer expansion. Harvesting chondrocytes via biopsies is limited by the amount of donor tissue and usually yields low cell numbers, which require extensive expansion in order to reach a suitable cell count. Unfortunately, monolayer expansion of

chondrocytes is associated with cell dedifferentiation, which is characterized by decreased proteoglycan synthesis and type II collagen expression [23]. Recently, stem cells have emerged as an alternative to autologous chondrocytes due to their availability and high capacity of expansion. Stem cells are pluripotent cells that can potentially be differentiated down various cell lineages under certain culture conditions. Sources for adult mesenchymal stem cells include bone marrow and adipose tissue. Mesenchymal stems cells are an intriguing cell source for tissue engineering cartilage, but the optimal differentiation conditions and long term efficacy of these cells have yet to be fully investigated.

Scaffolds

The scaffold provides a 3D environment and structure for the delivery of cells. Ideally the scaffold should be porous with an interconnected network to permit cell migration as well as nutrient and waste diffusion. The scaffold should also be biocompatible, biodegradable, and bioresorbable. Implantation of the scaffold must not cause any immunogenic response, nor should the degradation products from the scaffold yield any cytotoxic response. The time it takes for the scaffold to be replaced by ECM is also an important factor. A balance must be found since slow degradation will hinder new ECM production; whereas fast degradation may affect the structural stability of the scaffold. The surface of the scaffold should also promote cell attachment, proliferation and differentiation. This is usually done by enhancing the surface of the scaffold by adding cell-adhesion promoting molecules to the culture media. Currently, there is no particular scaffold that satisfies all of the numerous requirements, but the introduction of

new polymer and natural-based scaffolds, along with the use of bioactive molecules brings the creation of an ideal scaffold closer to reality.

Signaling Molecules

Cell signaling molecules bind to cells to create a biological response and include growth factors, adhesion proteins, and peptide sequences. These bioactive molecules are found throughout the body and are used in tissue engineering to induce, accelerate, and enhance tissue formation. The effect of various signaling molecules has been investigated through *in vitro* tissue engineering, which has allowed us to define the intensity, duration, and sequence of such molecules.

Several growth and differentiation factors concerning cartilage regulation have been investigated, such as the Transforming Growth Factor Beta Family (TGF-β), Bone Morphogenic Protein (BMPs), Cartilage Derived Morphogenic Protein (CDMP), Fibroblast Growth Factors (FGFs), and Insulin-like Growth Factor-1 (IGF-1). TGF-β isoforms are probably the most widely used growth factors with numerous studies exploring the TGF-β family's role in cartilage tissue engineering. TGF-β has been shown to induce chondrogenesis in adult mesenchymal stem cells[24], increase ECM synthesis [25], and enhance chondrocyte proliferation [26]. Growth factors are usually delivered as soluble factors in growth media for *in vitro* purposes, but have also been incorporated into scaffolds for timed-release after *in vivo* implantation. The surface of scaffolds can be modified by protein coating and peptide incorporation in order to enhance cell attachment and proliferation.

Although the role of growth factors has been shown to be very useful in cartilage tissue engineering, much still remains unknown about these signaling molecules. The

concentrations, dosage frequency, and affect of various cell sources must be further investigated. The long-term success of tissue engineering cartilage will depend on identifying the combinatory results and optimal application of different growth factors.

Motivation, Rationale, and Specific Aims

In 1743, William Hunter stated, "From Hippocrates down to the present age, we shall find, that an ulcerated cartilage is universally allowed to be a very troublesome disease, and that when destroyed, it is never recovered" [27]. Over two and a half centuries later, this statement still holds true today. When damaged, whether by trauma or disease, articular cartilage lacks the intrinsic ability for self-repair. If left untreated, injuries to cartilage can progressively become more severe and result in degenerative osteoarthritis. The natural repair response that arises from the disruption of subchondral bone results in the formation of fibrocartilage possessing inferior mechanical properties. Current therapies for articular cartilage repair have demonstrated favorable short term results, but are still unable to fully restore cartilage to its original state. Damage and degeneration of articular cartilage presents a major health issue worldwide. With increasing joint injuries in adolescents and the aging population, the need for a superior long-term treatment has become increasingly evident. The promise of tissue engineering has led to the development of a wide range of reparative and regenerative strategies; however, many challenges still remain. Further investigation into cell source, biomaterials, bioactive agents, and culture conditions are necessary in order to establish an ideal method for articular cartilage repair.

The goals of this study are to: 1) tissue engineer sizeable, scaffold-free cartilage to investigate the effect of Tissue Growth Technologies' CartiGen Bioreactor on the tissue

and 2) investigate chondrocyte and bone marrow-derived stem cell (BMSC) attachment to chitosan.

Specific Aim 1) Tissue engineer sizeable, scaffold-free cartilage to investigate the effect of Tissue Growth Technologies' CartiGen Bioreactor on the TE cartilage. Tissue engineering has looked towards bioreactors as a means for producing a suitable replacement tissue for cartilage. In this study, tissue engineered cartilage was created from porcine chondrocytes with the goal of improving the biomechanical and biochemical properties of the tissue through culture in the CartiGen bioreactor.

Specific Aim 2) Investigate chondrocyte and BMSC attachment to chitosan. Chitosan possesses interesting properties such as nontoxicity, biodegradability, and antimicrobial activity and has become a popular material for tissue engineering applications. Chesnutt et al. have developed composite co-precipitated chitosan/nano-calcium phosphate (CaP) microsphere-based scaffolds which support osteoblast attachment and growth, as well as overcome the limitations of mechanical strength and interconnected porosity seen in previous scaffolds. We extend this work to investigate the attachment of chondrocytes, BMSCs, and tissue engineered cartilage to chitosan/CaP microsphere-based scaffolds.

CHAPTER II

EFFECT OF A MECHANICAL STIMULATION BIOREACTOR ON SCAFFOLD-FREE TISSUE ENGINEERED CARTILGE

Introduction

Tissue engineering has emerged as a promising approach to develop tissue with identical properties to that of native articular cartilage. Generally, tissue engineering has involved the incorporation of cells into a scaffold; however, there has been a recent move towards a scaffold-free approach in order to avoid issues of biocompatibility, cell attachment, porosity, rate of bioresorption, cytotoxicity of degradation products, and stress-shielding [28]. Numerous approaches to forming scaffold-free constructs have been described: pellet culture [29], active tissue contraction [30, 31], transwells [32-35], custom molds [36-39], and agarose wells [40, 41]. Although scaffold-free engineered cartilage grown in static culture reliably develops the main features of articular cartilage, additional stimuli are required to increase the functional properties of the tissue. Two candidate stimuli are perfusion and dynamic unconfined compression, each of which has been shown independently to improve mechanical properties and enhance matrix synthesis of tissue engineered cartilage [42-47]. For example, Bian et al. demonstrated a significant increase in Young's modulus for adult canine primary chondrocyte-agarose constructs that were dynamically loaded in unconfined axial compression for three hours a day compared to free-swelling controls [42]. A study by Davisson et al. revealed an

increase in GAG synthesis and deposition by ovine articular chondrocyte constructs seeded on PGA scaffolds over nine days of continuous perfusion [46].

The C9-x CartiGen bioreactor from Tissue Growth Technologies (Fig. 2.1) is a means of simultaneously applying cyclic unconfined compression and perfusion to three-dimensional cell cultures and may be useful for producing functional engineered cartilage. The computer-controlled bioreactor system incorporates a motor, chamber, and peristaltic pump. The single axis stimulator has a maximum displacement of $\pm$ 5mm, maximum sinusoidal force of $\pm$ 20 N, and maximum frequency of 5 Hz. The chamber holds nine samples in individual wells. Medium is pumped from a reservoir and enters the bottom of each well through a porous metal disk. Having passed through and/or around the sample, the perfused media empties into a central well and returns to the reservoir. The objectives of this study were to: (i) describe the production of large, tissue engineered cartilage using a novel scaffold-free approach and (ii) determine the effect of perfusion and mechanical stimulation from the C9-x Cartigen bioreactor on the mechanical and biochemical properties of the tissue engineered cartilage.

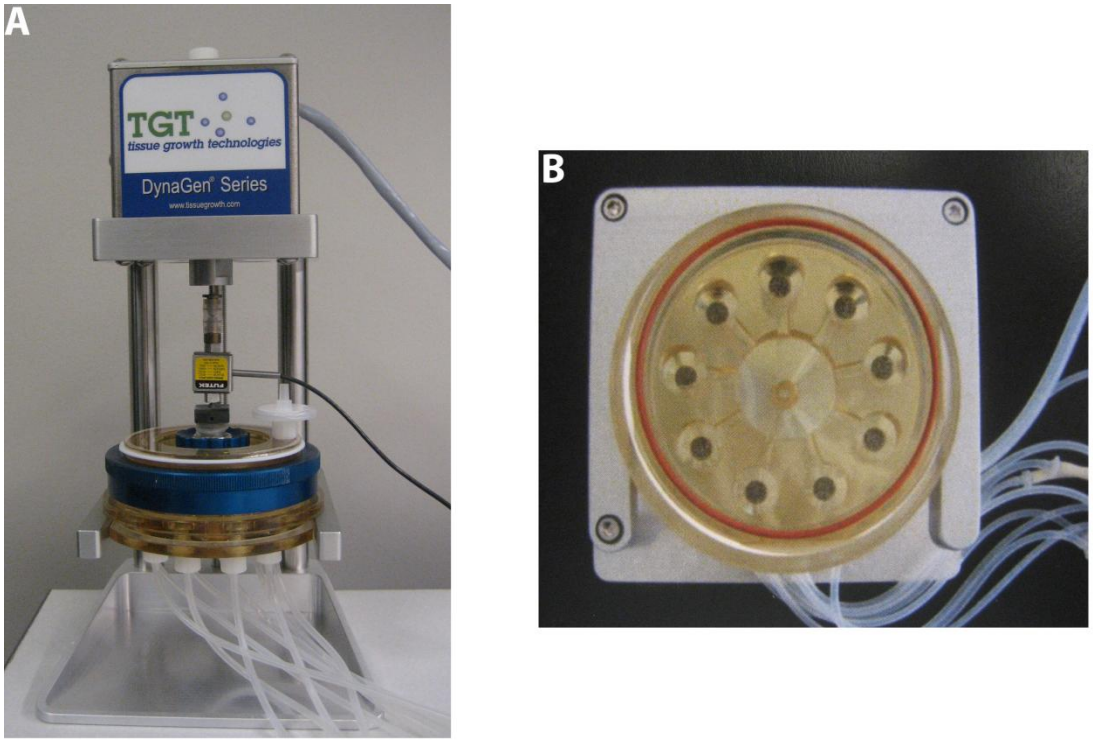

Figure 2.1 CartiGen C9-x bioreactor from Tissue Growth Technologies. (A) Front view showing chamber stand and single-axis stimulator. (B) Top view of chamber showing nine wells with porous bottoms.

Methods

Cell Source

Articular cartilage was aseptically harvested from the femoral condyles and femoral heads of 5 neonatal pigs. The cartilage was pooled, minced, and digested overnight in an incubator with 0.1% collagenase Type II in Dulbecco's Modified Eagle Medium (DMEM) containing 5% fetal bovine serum (FBS) and 1% antibiotic antimycotic solution (100 U/ml penicillin, 0.1 mg/ml streptomycin, 0.25 µg/ml amphotericin B). After enzymatic isolation, the cell solution was filtered through a 100µm filter to separate isolated chondrocytes from undigested material and the

chondrocytes were counted in a hemacytometer. Approximately 20 ml of a 2% molten agarose solution in DMEM was poured into 50 ml polypropylene centrifuge tubes and allowed to gel at 4°C. A suspension containing 6.5×10^7 cells was then added to each tube and centrifuged at 2000*g* for 3 minutes to create compact cell layers about 1 mm thick. The culture medium was initially high glucose DMEM containing 5% FBS, 1% FGF, and 1% antibiotic antimycotic solution. After 24 hours, it was replaced with defined chondrogenic medium: high-glucose DMEM, 1% ITS+Premix (6.25 μg/ml insulin, 6.25 μg/ml transferring, 6.25 μg/ml selenious acid, 1.25 mg/ml bovine serum albumin, 5.35 μg/ml linoleic acid), 0.1 μM dexamethasone, 50 μg/ml ascorbate-2 phosphate, 1 mM sodium pyruvate, 40 μg/ml L-proline, 1% antibiotic antimycotic solution, and 10 ng/ml of TGF-β3. The constructs remained in the tubes for 10 days with defined chondrogenic medium, which was replaced every 3 or 4 days.

Static and Bioreactor Culture

After the 10-day consolidation phase the constructs were firm enough to handle gently with forceps and cut with a scalpel. Each construct was removed from its tube and an 8mm diameter disk was cored from the center using a biopsy punch. Six 8mm disks, along with their concentric rings, were transferred to a six well plate, which had been coated with a thin layer of agarose. These control constructs were incubated in defined chondrogenic medium under static, free swelling conditions for the duration of the study. The medium was changed twice a week. Nine disk-ring pairs were placed into each well of the CartiGen chamber. They were positioned centrally within each well so that the inner disk was coaxial with the 6 mm diameter smooth, impermeable loading head. The

disks and concentric rings were subjected to constant surface perfusion with defined chondrogenic medium at a flow rate of 0.5 mL/min for the duration of the four week culture in the bioreactor. During the first week of culture in the CartiGen bioreactor, the loading heads were stationed several millimeters above the disks and no mechanical stimulation was applied. After the first week, disks were subjected to 1.0 Hz sinusoidal unconfined compression under load control for four hours a day, five days a week, beginning with a load of 0.5 N and increasing to 10 N and 20 N the second and third weeks, respectively. The loading heads were lifted several millimeters off of the constructs during the rest periods. During loading, the total force applied to all nine samples, as well as the displacement of the loading frame, were recorded for 10 seconds at the beginning of the third hour of loading. Dynamic compressive stiffness was calculated as the peak-to-peak force divided by the peak-to-peak displacement. Throughout the consolidation and bioreactor phases, the cultures were maintained in a standard tissue culture incubator at 37°C and 5% CO_2.

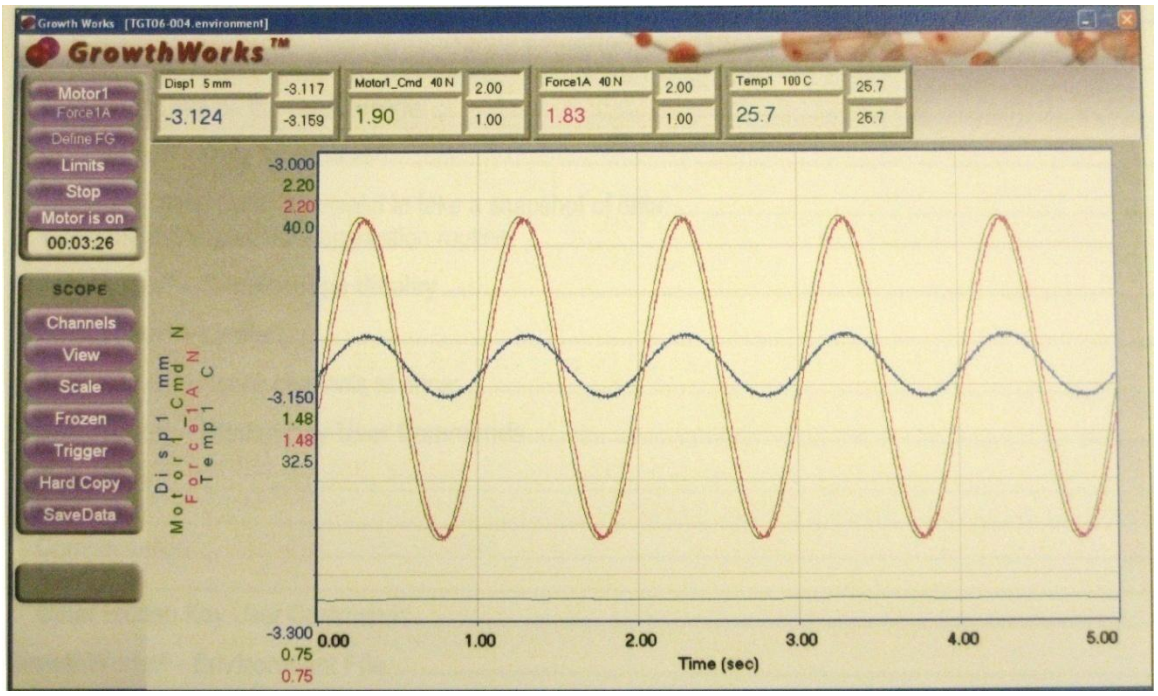

Figure 2.2 GrowthWorks software user interface.

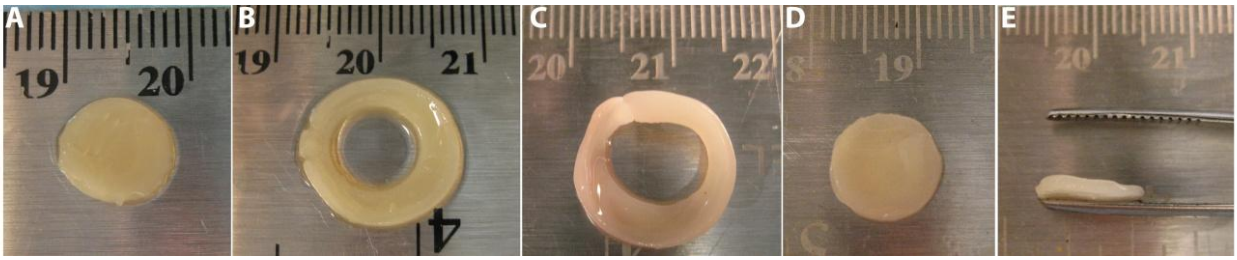

Figure 2.3 Gross appearance of static, perfused and loaded constructs. (A) static disk, (B) static ring, (C) perfused ring, (D) loaded disk, and (E) loaded disk thickness

Biomechanical Analysis

All biomechanical analyses were performed using the Biosyntech Mach-1 testing system (Fig. 2.4). For unconfined compression tests, samples were transferred to a stainless steel dish containing room temperature phosphate-buffered saline (PBS).

Contact with each specimen was established by preloading to 10 g at 10 μm/s and holding at this position until the force equilibrated. The unconfined compression test consisted of four displacement ramps of 5% strain, each of which was followed by stress relaxation to equilibrium. Force was normalized to sample cross-sectional area and the equilibrium stresses were plotted against the applied strain. Equilibrium compressive modulus was calculated as the slope of the best-fit line through these points. The stress relaxation protocol was followed by a dynamic test, which consisted of a sinusoidal profile with 3% strain amplitude at 0.01 Hz for 2 cycles, 0.025 Hz for 3 cycles, 0.25 Hz for 10 cycles, and 1 Hz for 20 cycles. Using data from the cycles of each frequency, the dynamic modulus was calculated as the peak-to-peak stress divided by peak-to-peak strain.

Following the unconfined tests, samples were allowed to recover for at least 1 hour before undergoing confined compression testing. For the confined compression tests, a 3.75 mm core of each sample was collected using a 3.75 mm punch. The disks were placed into a custom polycarbonate holder consisting of a porous, stainless steel base (Fig. 2.5) and were compressed with a solid stainless steel indenter. The confined compression test consisted of one displacement ramp to 20% strain followed by stress relaxation to equilibrium. Aggregate modulus and hydraulic permeability were determined by curve fitting the results to the linear biphasic theory of Mow et al. [48] using the stress relaxation solution presented by Soltz and Ateshian [49].

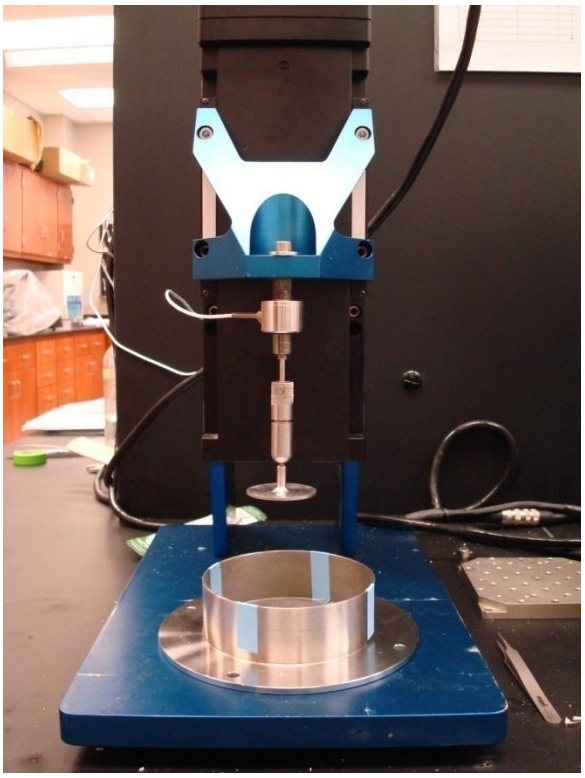

Figure 2.4 Biosyntech Mach-1micromechanical testing system. Configuration shown is utilized for unconfined compression tests.

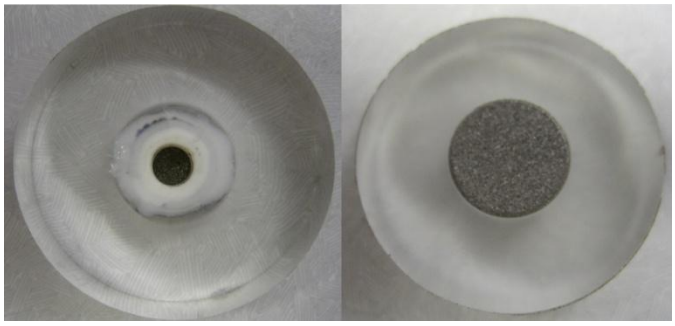

Figure 2.5 Custom polycarbonate well with porous bottom used for confined compression tests.

Biochemical Analysis

One-fourth of each disk was digested in 1% papain and 50 mM sodium acetate (pH 6) at 60° C overnight. The total DNA content of the digestate was measured using the Hoescht method (Sigma DNA-QF kit). Fluorescence intensity was measured using a Vicam Series-4 Fluoremeter (Vicam, Milford, MA). Total GAG content from the same digestate was quantified using the Blyscan Glycosaminoglycan Assay kit (Biocolor, Newtonabby, Northern Ireland), based on dimethyl methylene blue binding. The remaining half of each disk, designated for collagen content, was incubated at 4° C for 48 hours in 0.05 M acetic acid containing 0.5 M NaCl (pH 3) and pepsin (10 mg/mL). Pancreatic elastase (1 mg/mL dissolved in 1x TBS, pH 7.8-8.0) was added to the digestate and mixed at 4° C overnight on a rotator rocker. Total collagen was determined by the Sircol Assay (Biocolor) with absorbance at 540 nm measured using a BioTek µQuant Microplate Spectrophotometer (BioTek Insturments, Winooski, VT).

Gross Morphology and Histology

Digital photographs were taken to record gross morphology and to measure the diameter of each construct using Image J analyzing software (Image J 1.41, National Institutes of Health, USA). Thickness for each construct was determined by finding contact for each disk under a 10 g compressive load using the Mach-1 Micromechanical testing system (Mach-1™ Motion, Bio Syntech Canada, Inc, Quebec, Canada).

One-fourth of each construct was fixed in 10% neutral buffered formalin, embedded in paraffin, and sectioned (10 µm). Sections were stained with toluidine blue to evaluate proteoglycan concentration.

Results

Gross Morphology and Histology

Centrifugation (2000*g*, 3 min) onto agarose bottoms of 50 mL tubes compacted cells into a relatively even layer about 1 mm thick covering the diameter of the tube. After one week of static culture in the tubes, the constructs were firm and glossy, could be cleanly cut by a biopsy punch (Fig. 2.6A), and could be easily handled and manipulated with forceps (Fig. 2.6B). Although thickness increased in all groups from the initial ~1 mm, there was no significant difference in thickness between the groups after 5 weeks of culture (Fig. 2.7).

Histological evaluation shows an intense staining with toluidine blue in all constructs, indicating an extracellular matrix rich in proteoglycans. However, higher staining intensities of toluidine blue can be seen in the perfused and loaded groups compared to the static group (Fig. 2.8).

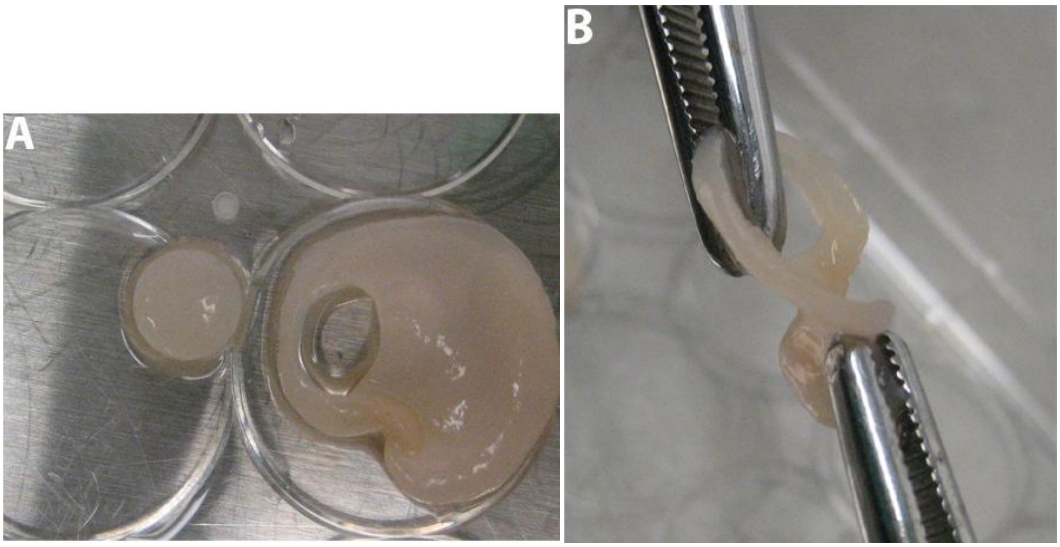

Figure 2.6 Gross appearance of tissue engineered, scaffold-free cartilage disks. (A) Disk cut by 6 mm biopsy punch. (B) Torsion of disk with forceps demonstrates ease of handling after 5 weeks culture.

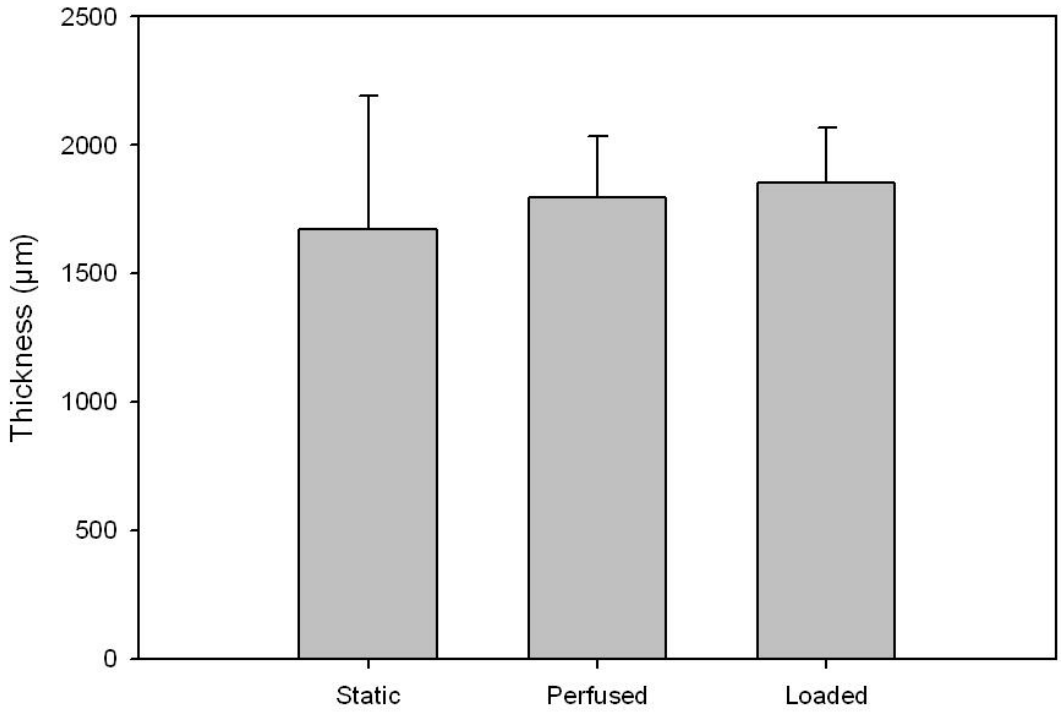

Figure 2.7 Thickness of engineered, scaffold-free cartilage disks after 5 week culture period.

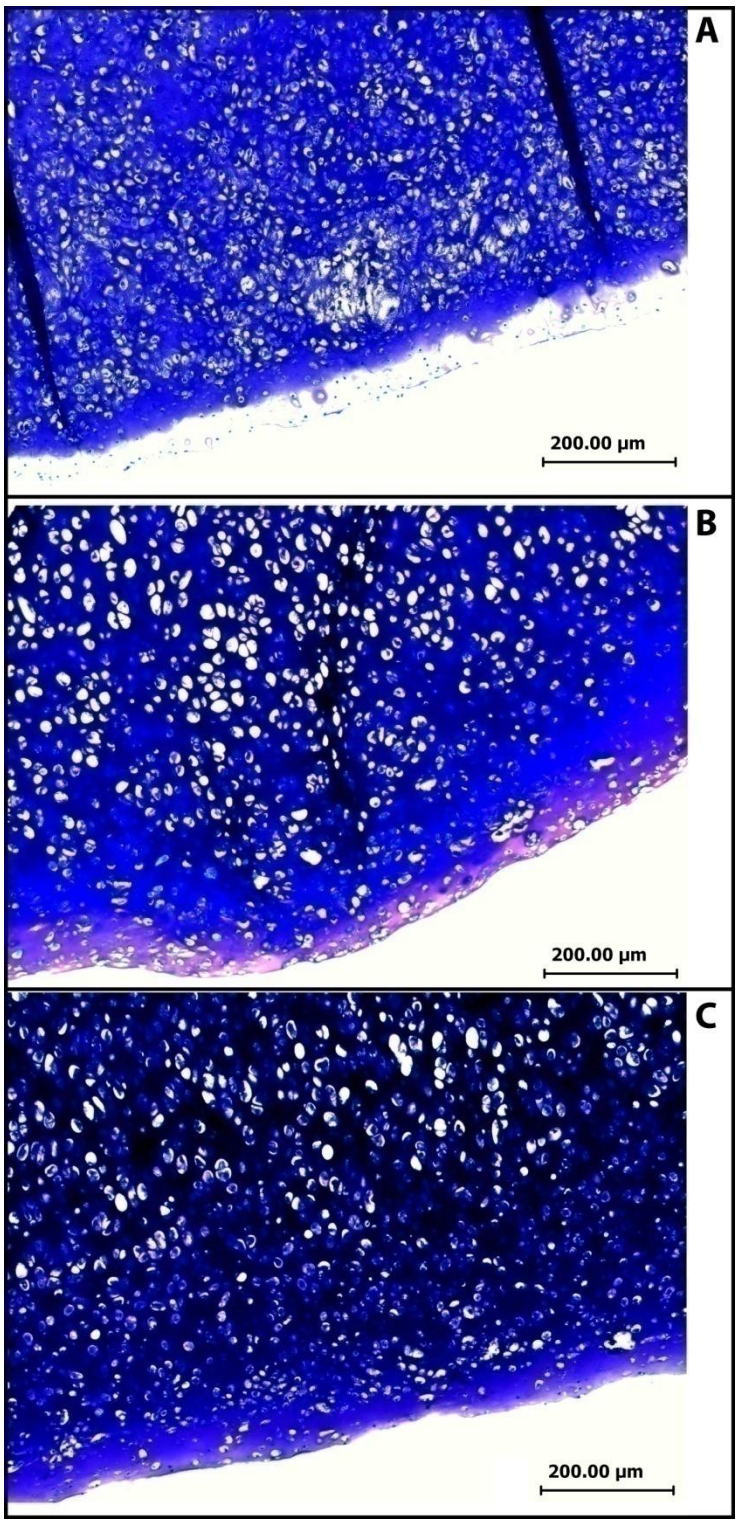

Figure 2.8 Histological sections of (A) static, (B) perfused, and (C) loaded constructs stained with toluidine blue.

Biochemical Analysis

All numerical results are expressed as the mean ± SD. Total collagen content for native porcine cartilage and the three experimental groups is shown in Figure 2.9. Collagen content for the static (13.0902 ± 4.4965), perfused (16.6458 ± 6.8721), and loaded (14.1936 ± 3.6011) group was much lower than the native group (56.4460 ± 13.9081). The amounts of collagen in the experimental groups were similar and did not show any significant difference. Total GAG content for the experimental groups and native porcine cartilage is shown in Figure 2.10. GAG content was much higher in the perfused (79.4149 ± 21.9862) and loaded (82.6923 ± 18.4827) groups than the static (47.3069 ± 17.4817) and native (64.1732 ± 5.3124) groups. Qualitative and quantitative analysis of GAG content reveals a beneficial effect from culture in the bioreactor compared to static culture. GAG content increased almost two fold in bioreactor cultured constructs as opposed to statically cultured constructs. After five weeks of culture in the bioreactor, the GAG/dw in the perfused and loaded groups exceeded that of native porcine articular cartilage.

The DNA content was similar among the three experimental groups, but there was no significant difference between static, perfused, or loaded groups (Fig. 2.11). The DNA content was higher in the three experimental groups than in the native group but the differences were not statistically significant.

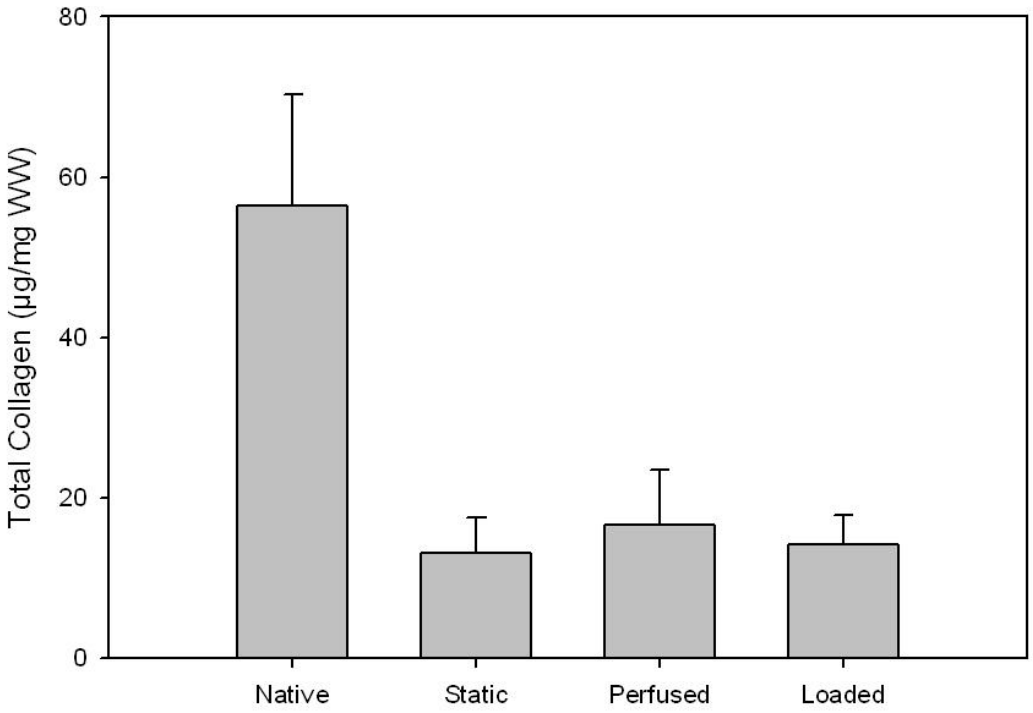

Figure 2.9 Total collagen content in engineered scaffold-free disks.

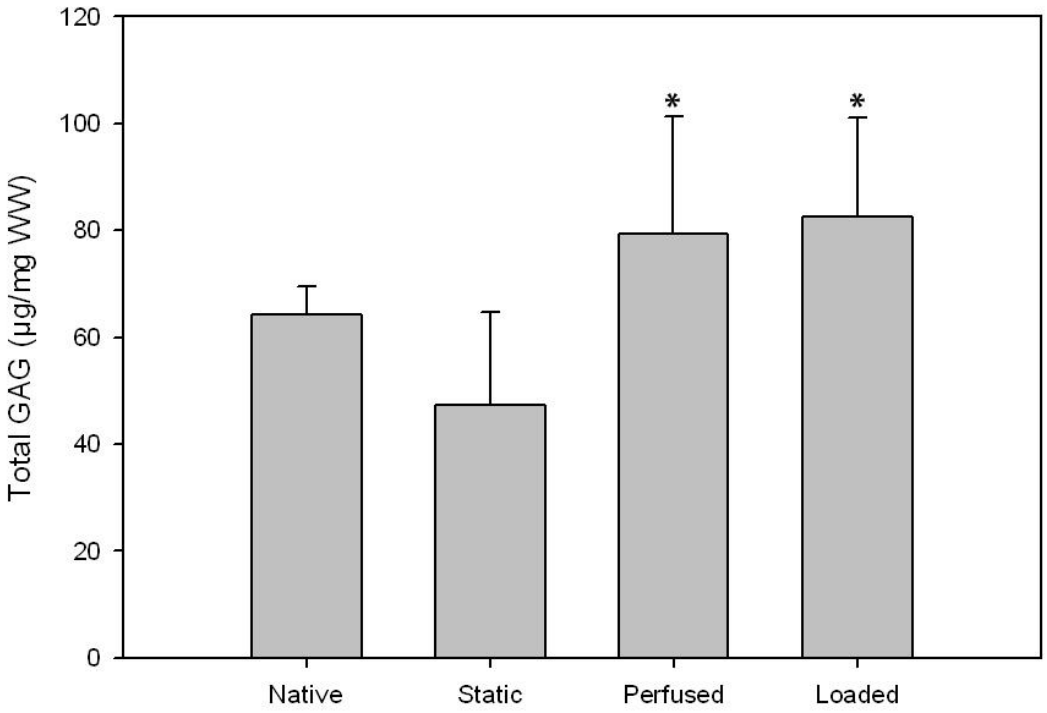

Figure 2.10 Total GAG in engineered scaffold-free disks. (*) indicates significant statistical difference vs. static ($p < 0.001$)

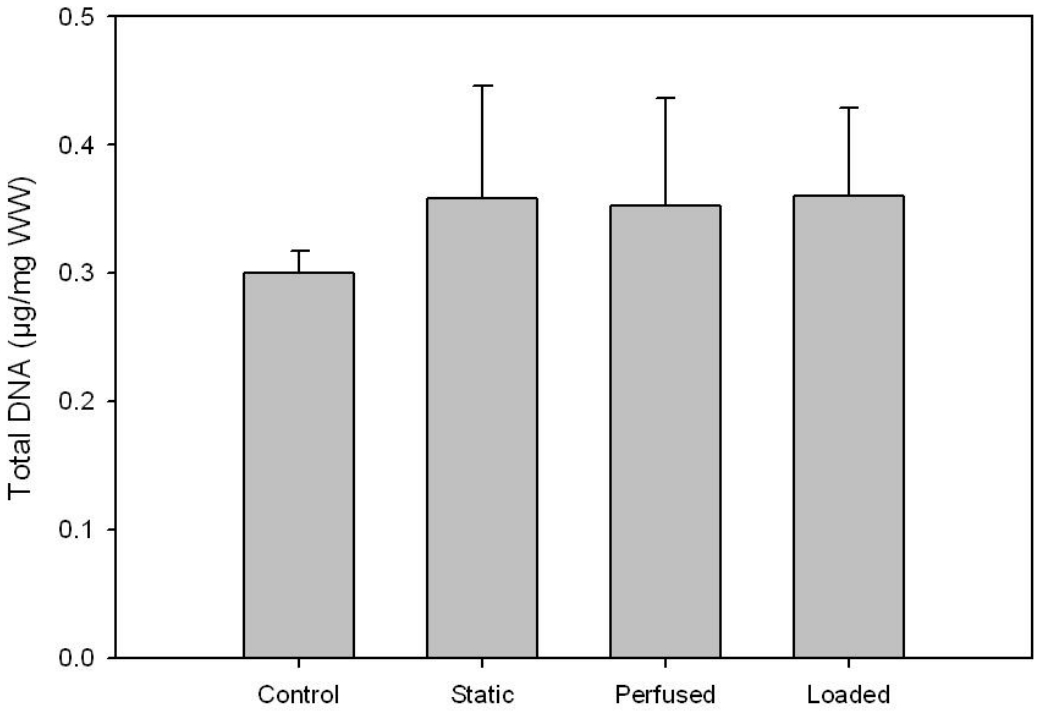

Figure 2.11 Total DNA in engineered scaffold-free disks.

Biomechanical Analysis

During culture in the bioreactor, the compressive dynamic stiffness was calculated for only the loaded constructs based on the recorded peak-to-peak force and peak-to-peak displacement of the loading platens during periods of loading (Fig. 2.12). The compressive dynamic stiffness of the loaded constructs not only increased each week, but exhibited an increase in a linear fashion.

After removal from culture, all constructs underwent unconfined compression tests to calculate dynamic modulus. Although both perfused (53.5394 $\pm$ 33.7858 N/mm) and loaded (17.9215 $\pm$ 12.3923 N/mm) groups attained a higher dynamic modulus than

the static group (5.2230 $\pm$ 2.4777 N/mm), only the perfused group was significantly higher (Fig. 2.13). However, both perfused and loaded groups had significantly higher equilibrium compressive moduli than the static group (Fig. 2.14).

The equilibrium compressive modulus for the static group only reached 5.2943 $\pm$ 2.7014 MPa, whereas the perfused group reached 67.1766 $\pm$ 35.3546 MPa and the load group reached 45.2495 $\pm$ 16.6148 MPa. There was no significant difference in aggregate modulus between the three groups (Fig. 2.15). The aggregate modulus for the loaded group was only slightly higher than static, while the aggregate modulus of the perfused group reached only about 50% that of the static group. Both perfused and loaded groups attained a significantly lower hydraulic permeability than the static group (Fig. 2.16). The hydraulic permeability for static ($3.0993E10^{-14}$ $\pm$ $1.7239E10^{-14}$ m^4/Ns), perfused ($8.8478E10^{-15}$ + $4.2912E10^{-15}$ m^4/Ns), and loaded ($3.6447E10^{-15}$ + $1.6474E10^{-15}$ m^4/Ns) groups was lower than the hydraulic permeability previously found for neonatal articular cartilage ($12.7E10^{-14}$ m^4/Ns) [32]. The average percent stress relaxation of the static group was 83.693 $\pm$ 4.9157 %, while the average percent stress relaxation of the perfused and loaded groups were significantly lower at 54.130 $\pm$ 6.527 % and 62.288 $\pm$ 8.059 % respectively (Fig. 2.17). Both the perfused and loaded groups had stress relaxation curves that were statistically different from the static group (Fig. 2.18).

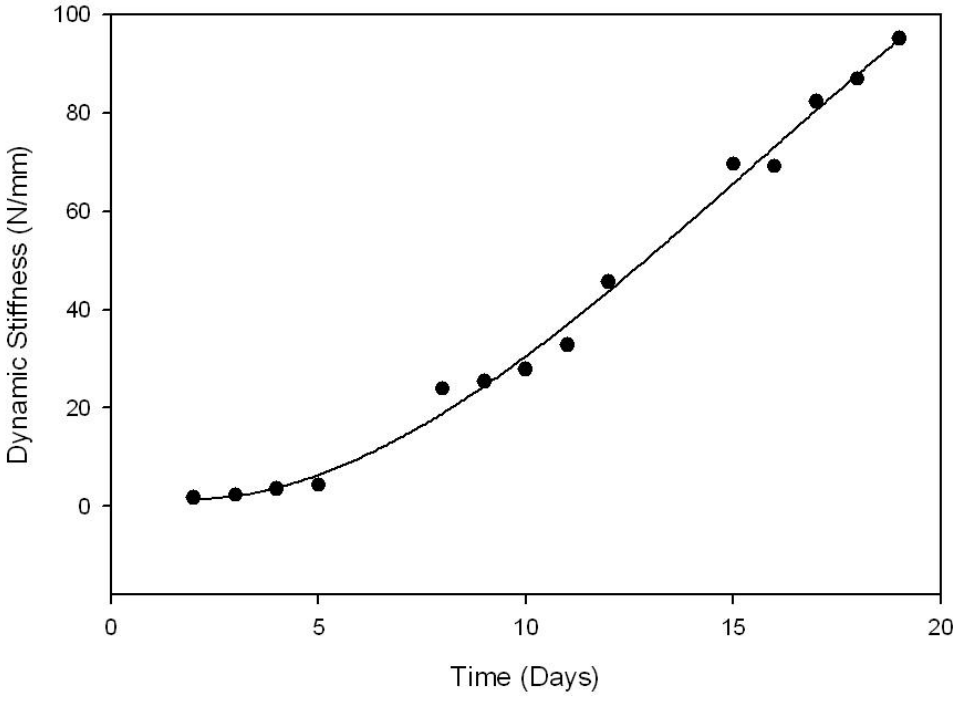

Figure 2.12 Dynamic stiffness of engineered scaffold-free cartilage calculated from data obtained during loading in the CartiGen bioreactor.

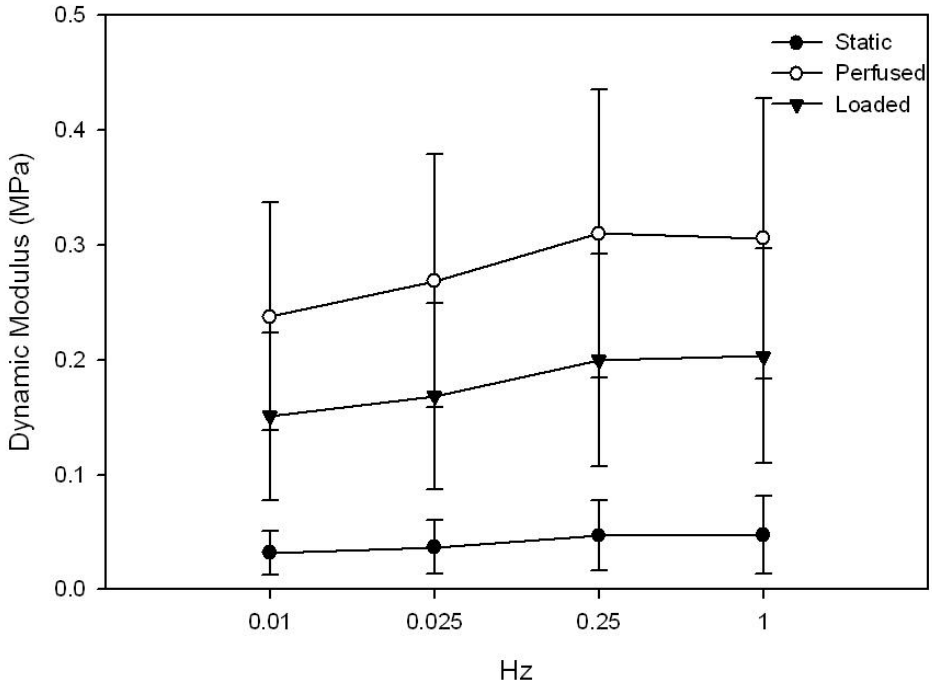

Figure 2.13 Dynamic modulus of engineered scaffold-free cartilage obtained from unconfined compression tests.

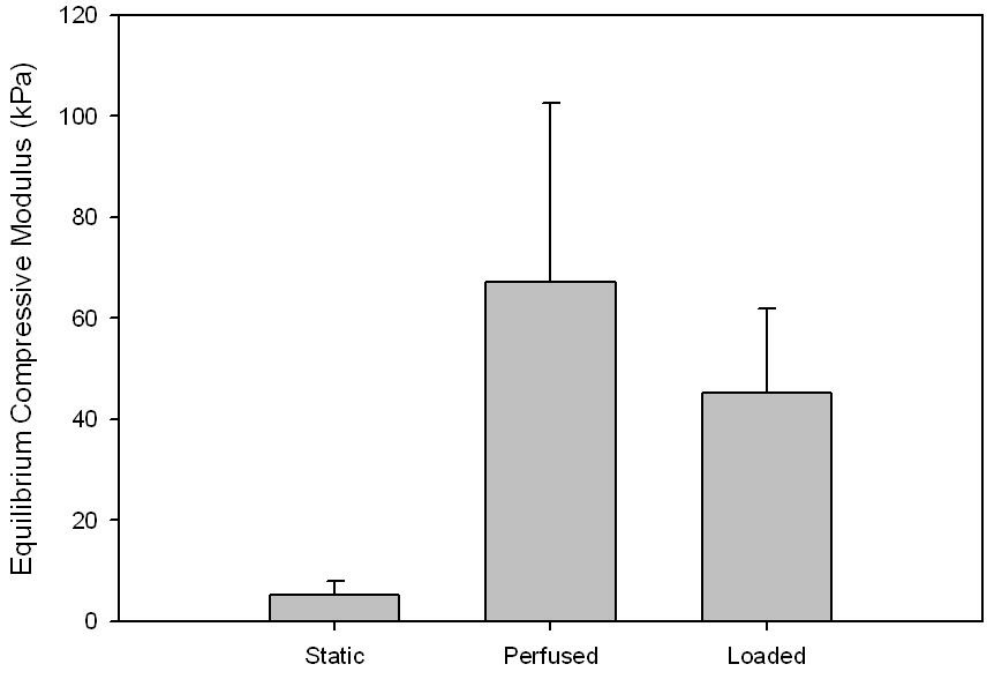

Figure 2.14 Equilibrium compressive modulus of engineered scaffold-free cartilage determined from unconfined stress relaxation tests. (*) indicates significant statistical difference vs. static ($p < 0.001$)

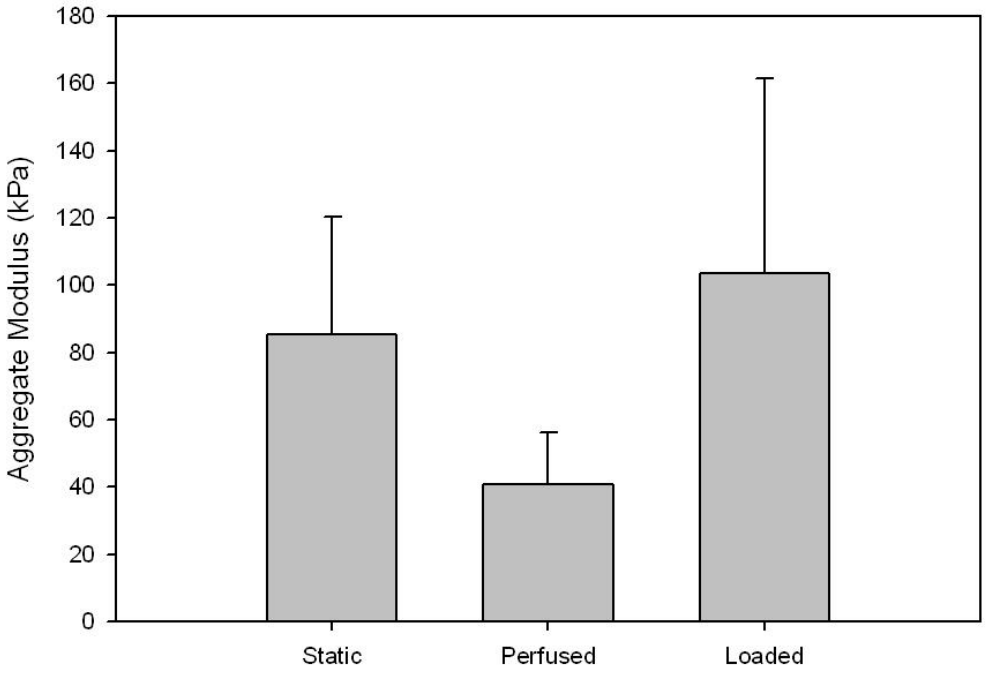

Figure 2.15 Aggregate modulus of engineered scaffold-free cartilage determined by curve fitting results from confined compression tests to the stress relaxation solution of Soltz and Ateshian.

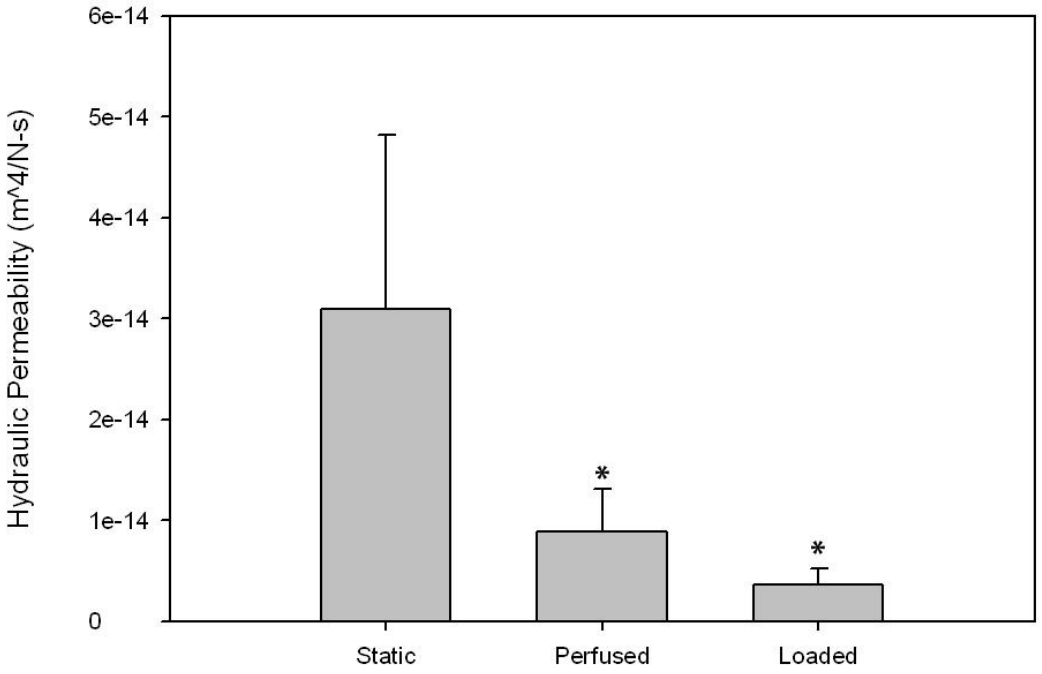

Figure 2.16 Hydraulic permeability of engineered scaffold-free cartilage determined by curve fitting results from confined compression tests to the stress relaxation solution of Soltz and Ateshian. (*) indicates significant statistical difference vs. static ($p < 0.001$).

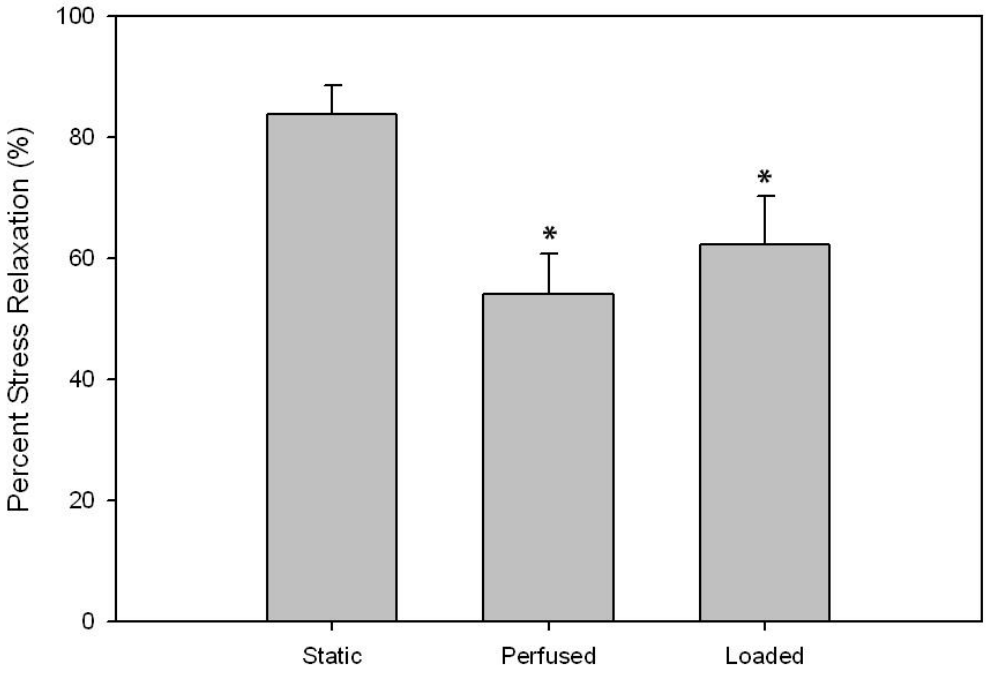

Figure 2.17 Percent stress relaxation of engineered scaffold-free cartilage. (*) indicates significant statistical difference vs. static ($p < 0.001$).

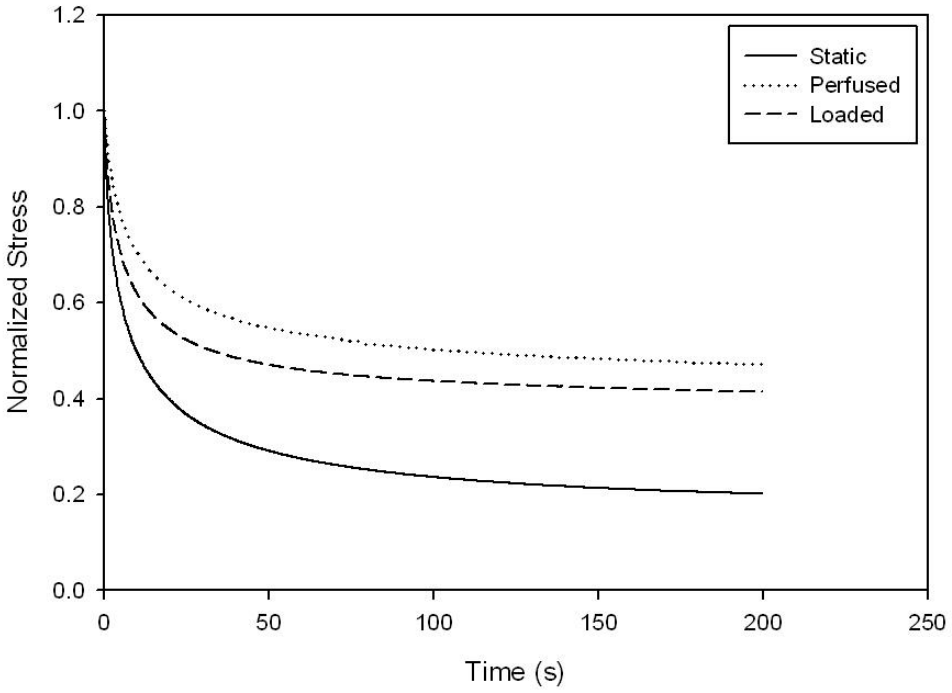

Figure 2.18 Stress relaxation properties of engineered scaffold-free cartilage. Note the different mean stress relaxation curves of the three experimental groups.

Discussion

In this study, we introduce a novel method for producing sizable tissue engineered cartilage from neonatal porcine chondrocytes utilizing a scaffold-free approach. We also investigate the effects of culturing these tissue engineered constructs in a C9-x CartiGen bioreactor from Tissue Growth Technologies. The nine constructs were mechanically stimulated based on load control, which more closely mimics physiological conditions more so than displacement control. The gross and histological appearances, biochemical content, and mechanical properties of constructs cultured in a C9-x CartiGen bioreactor were compared to constructs cultured statically and to native porcine cartilage. Our results demonstrate that the CartiGen bioreactor is able to enhance both biochemical and

mechanical properties of tissue engineered cartilage derived from neonatal porcine chondrocytes.

The total DNA content was found to be similar among the static, perfused, and loaded groups. Since total DNA content from bioreactor cultured constructs did not differ from static cultured constructs, this suggests that the bioreactor did not promote or enhance further cell proliferation over static culture conditions.

Although constructs cultured in the bioreactor achieved GAG levels higher than native tissue, the constructs exhibited a deficiency in collagen. This high GAG content along with low collagen content in tissue engineered cartilage has been reported by numerous studies [50-52]. According to Riesle, the low collagen content could possibly be attributed to enzymatic degradation as a result of fewer mature collagen cross-links in tissue engineered cartilage [53]. In a comparative study between immature and mature rabbit articular cartilage, Julkunen et al. determined that the collagen network does not reach mature properties until around the age of three months [54]. After five weeks of culture in the bioreactor, the collagen/dw in all groups reached about 33% that of native porcine articular cartilage.

It has been well documented that glycosaminoglycans contribute to the compressive properties of articular cartilage. The equilibrium compressive modulus of bioreactor cultured groups was much higher than statically cultured groups and can be attributed to the increase in GAG deposition in the perfused and loaded groups. The higher GAG concentration in constructs cultured in the bioreactor is also reflected in the lower permeability of those groups. The lower permeability, in conjunction with increased GAG content, resulted in a higher dynamic stiffness in perfused and loaded

groups than in the static group. The permeability also directly affects the maximum peak stress each construct can attain during the loading segment of stress-relaxation tests. Therefore, a lower permeability allows the construct to support higher peak stresses. As the results indicate, the perfused and loaded groups had significantly lower permeability and significantly lower stress relaxations by percentage. Surprisingly, the aggregate modulus for the perfused and loaded groups was not higher than the static group. The average aggregate modulus for the loaded group was only slightly higher than static, whereas the aggregate modulus of the perfused group reached only about 50% that of static. This result may be due to the lack of collagen content in our tissue engineered constructs. Earlier studies have shown the aggregate modulus to be dependent on GAG content [55], but more recent studies have shown the aggregate modulus is also correlated with collagen content [56, 57]. Mauck et al. observed that the aggregate modulus of tissue engineered cartilage had an even stronger dependence on collagen content as opposed to GAG content [57].

Our results clearly indicate an enhancement of properties in perfused and loaded groups over the static group; however, there is no evidence from our study that suggests the perfused or loaded condition produced a more superior tissue than the other. Both mechanical stimulation and perfusion have been shown to improve the quality of tissue engineered cartilage. Dynamic compression stimulates chondrocyte metabolism and increases matrix synthesis, thus improving the mechanical properties of tissue engineered cartilage [44, 50, 57-61]. Perfusion has been linked to an accumulation of ECM in tissue engineered cartilage by inducing shear stress on constructs and allowing for constant nutrient supply and waste removal [46, 62, 63]. We expected to see an increase in

biomechanical and biochemical properties from the perfused group compared to the loaded group; however, there was no significant difference between the two groups. The nine loading platens do not function independently from another, but rather all nine are rigidly attached to a single, unidirectional stimulator. Therefore, it is difficult to ensure that all constructs are receiving precisely the same load due to differences in thickness between constructs. The majority of the load could possibly be borne by any number of the constructs. Any additive effects related to mechanical stimulation may also have been negated by direct contact from the impermeable loading platen which has been shown to reduce synthesis of matrix products by disrupting nutritional transport to the constructs [64].

In order to improve this method of tissue engineering, future studies should involve the use of a more clinically relevant cell source such as adult chondrocytes or bone-derived mesenchymal stem cells. Utilizing a more mature cell source would introduce additional variables such as age and cell passaging. Culture duration, initial loading, and an optimized loading regime must also be further investigated in order to produce tissue, which possesses sufficient properties for implantation.

Our study demonstrates that sizeable tissue engineered cartilage can be produced from primary porcine chondrocytes using a scaffold-free centrifugation method. Furthermore, the biomechanical and biochemical properties of these constructs are enhanced via culture in a C9-x CartiGen bioreactor capable of applying mechanical stimulation and constant perfusion. The ability to produce sizeable tissue engineered cartilage possessing functional properties approaching that of native tissue serves as progress towards future cartilage regeneration.

CHAPTER III

INVESTIGATIONS INTO CHITOSAN FOR CARTILAGE TISSUE ENGINEERING

Introduction

Chitosan is a deacetylated derivative of chitin, which is the second most abundant biopolymer behind cellulose. Chitin is found in the exoskeleton of marine crustaceans and is produced by the seafood industry as industrial waste. Chitosan is a linear polysaccharide composed of glucosamine and N-acetyl glucosamine units linked by β(1-4) bonds. The ratio of glucosamine to N-acetyl glucosamine determines the degree of deacetylation (DD) of the chitosan. Chitosan's molecular weight can range from 50-1000 kDa and its DD can range from 50-90%, depending on the source and method of preparation [31]. Chitosan has been a widely investigated biomaterial due to its nontoxicity, biodegradability, enhancement of wound healing [65], antimicrobial activity [66], and ability to be molded into various forms [67, 68]. Hydroxyapetite (HA) is one of the major constituents of bone and has been widely used in orthopedic surgery due to its biocompatibility and osteoconductivity [69, 70].

Chitosan and HA have been investigated as possible scaffold biomaterials for tissue engineering cartilage and bone, respectively. When used alone, chitosan lacks the mechanical properties required for load bearing activities, whereas HA is difficult to shape due to its hardness and brittleness. A combination of both biomaterials could provide an ideal scaffold for the repair of osteochondral defects, where both the articular

cartilage and underlying bone are damaged. It has been shown that the incorporation of HA into polymer matrices has increased the bone-binding capability of the polymer [71, 72]. Previous preparation methods have involved mixing HA powder in chitosan solution [73] and coating a chitosan sheet with HA particles [74]. These methods resulted in inhomogeneous composites with poorly integrated HA in the chitosan, however co-precipitation methods have resulted in homogenous HA/chitosan composites [67, 75, 76].

Chesnutt et al. developed composite co-precipitated chitosan/nano- calcium phosphate (CaP) microsphere-based scaffolds which support osteoblast attachment and growth, and overcome the limitations of mechanical strength and interconnected porosity seen in previous scaffolds [77]. In this study, the work of Chesnutt et al. was extended to investigate the attachment of tissue engineered cartilage to chitosan/CaP microsphere-based scaffolds. The first objective was to investigate whether the formation of CaP crystals on the chitosan was an immediate process that occurred after immersing the chitosan in the precipitation solution or a gradual process that required soaking the chitosan in the precipitation solution over a period of time. Next, a pilot study was done to assess the chitosan's ability to support the attachment of cells using porcine bone marrow–derived mesenchymal stem cells (BMSCs). We followed with additional studies to evaluate methods for creating a biphasic scaffold consisting of a layer of scaffold-free cartilage attached to a porous chitosan scaffold using transwells and 15-mL centrifuge tubes.

Methods

Formation of Calcium Phosphate (CaP) Crystals

Chitosan Disc Fabrication

To prepare the chitosan solution, 3.57 g of 78.7% DDA chitosan powder (Vanson, Remond, WA) was dissolved in 84 mL 2 wt% acetic acid. Ten mL of 1 M $CaCl_2$ in 2% acetic acid and 6 mL 1 M NaH_2PO_4 in 2% acetic acid was added to the chitosan solution. The precipitation solution was composed of 20% NaOH, 30% methanol, and 50% water (pH = 13). Enough precipitation solution was added to a 100 mL beaker to coat the bottom and sides. Ten mL of chitosan solution was added to the beaker. Precipitation solution was added via spray bottle to ensure the initial gelling of the top surface of the chitosan. The chitosan discs were allowed to soak in the precipitation solution for either 10 minutes or 24 hours. After soaking, the chitosan discs were washed until a neutral pH was reached.

For the control, 3.57 g of 78.7% DDA chitosan powder (Vanson, Remond, WA) was dissolved in 100 mL of 2 wt% acetic acid. This chitosan solution did not include $CaCl_2$ and NaH_2PO_4, therefore preventing formation of any calcium phosphate crystals. Once again, enough precipitation solution was added to a 100 mL beaker to coat the bottom and sides. Ten mL of the control chitosan solution was added to the beaker. Precipitation solution was added via spray bottle to ensure the initial gelling of the top surface of the chitosan. The chitosan discs were allowed to soak in the precipitation solution for 24 hours. After soaking, the chitosan discs were washed until a neutral pH was reached as described previously.

Transmission Electron Microscopy

Samples of control chitosan, chitosan soaked for 10 minutes, and chitosan soaked for 24 hours were trimmed and faced for cutting by an ultra-microtome (Reichert Junt Ultracut E). Thin sections (75 nm) were cut and then collected on a copper grid. The sections were viewed with a JEOL JEM-100CXII TEM scope at 60-80kV.

BMSC Attachment to Microspheres

Chitosan Microsphere Fabrication

Chitosan solution was prepared as described previously. The chitosan solution was placed in a 30-mL syringe fitted with a 21-g needle. The syringe was placed in a syringe pump and dripped into a precipitation solution with constant stirring. An air line was attached to the syringe to force the chitosan solution off of the tip of the needle. The size of the chitosan microspheres could be fabricated to a desired size by controlling the air flow. The chitosan solution immediately formed into solid beads after being dripped into the precipitation solution. The microspheres were left in the precipitation solution for 24 h to allow crystalline CaP to develop. The microspheres were then washed in numerous changes of deionized water until they reached a neutral pH (7.0-7.5). The pH was measured with a pH meter after each change of DI water.

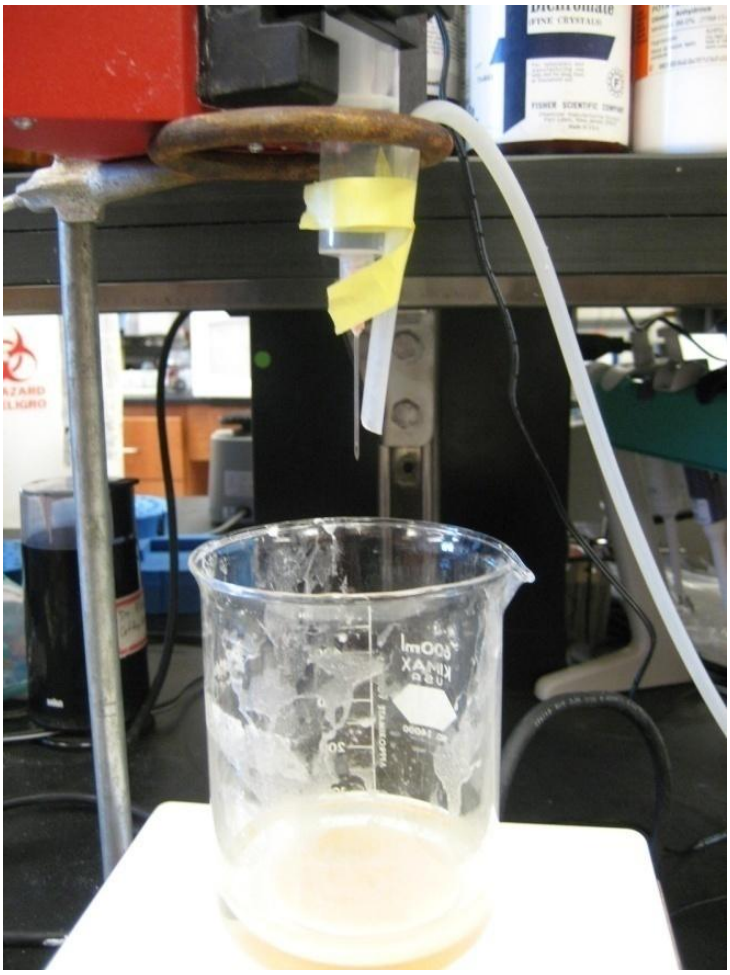

Figure 3.1 Setup for chitosan microsphere formation. Chitosan solution was dripped from the needle by a syringe pump. Air line was attached to the syringe to control the size of the microspheres based on air flow.

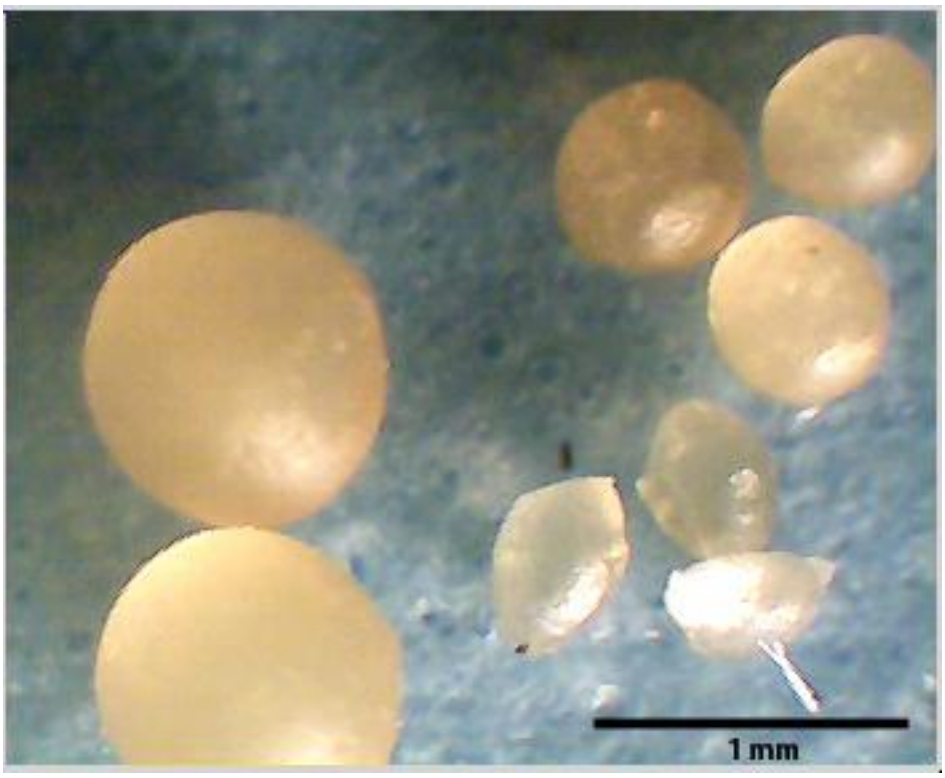

Figure 3.2 Image of various sizes of microspheres taken by a dissection microscope.

Cell Source and Culture

Bone marrow derived mesenchymal stem cells (BMSCs) were obtained from the femur and tibia of neonatal pigs. Working under aseptic conditions, the femurs and tibias were removed and cleaned of any connective tissue. Bones were briefly rinsed in 10% bleach, washed in 70% ethanol, and then allowed to dry in a sterile Pyrex dish on ice. The bones were cut in half and each half was placed in a syringe with the open end of the bone pointed downward. Each syringe was placed in a 50 ml centrifuge tube and then centrifuged for 10 minutes at 200 g to extract the marrow from the bone. Centrifugation causes the bone marrow to pass through the syringe and collect in the bottom of the 50 mL centrifuge tube. Syringes and bones were removed and bone marrow was pooled.

The bone marrow was then pipetted into culture flasks and allowed to incubate overnight. Since BMSCs are substrate dependent, they adhere to the flasks. Rinsing the flasks the following day will remove the non-adherent blood cells, leaving a population of BMSCs. The porcine BMSCs were detached using 0.25% trypsin-EDTA and recovered from the flasks. A cell suspension containing 500,000 BMSCs was added to a sterile microcentrifuge tube containing two or three chitosan microspheres and allowed to attach for 24 hours in a standard tissue culture incubator at 37°C and 5% CO_2.

Scanning Electron Microscopy

Samples were fixed in 2.5% glutaraldehyde, dehydrated in a graded ethanol series, and chemically dried with Hexamethyldisilazane (HMDS). After drying, samples were placed with desiccant until mounting. Samples were mounted to stubs using carbon tape and sputter coated with gold-palladium. The samples were viewed with a JEOL JSM-6500F at 5 kV. The surface of the chitosan microspheres were examined visually for cell attachment and images were recorded. Unseeded chitosan was also imaged to examine surface topography and to serve as a control for comparison.

Biphasic Constructs (Transwell Model)

Scaffold Fabrication

Chitosan microspheres were created as described earlier. The microspheres were then packed into 6.5 mm diameter transwells and fused into cylindrical plugs by washing with 1% acetic acid for 20 seconds and placed in deionized water for rinsing. The cylindrical scaffolds were removed from the deionized water and allowed to dry for 24 h.

Dry scaffolds were sterilized by ethylene oxide. Before cell seeding, scaffolds were rehydrated in medium containing 5% fetal bovine serum (FBS) and 1% antibiotic antimycotic solution (100 U/ml penicillin, 0.1 mg/ml streptomycin, 0.25 μg/ml amphotericin B) for 24 hours to coat the scaffolds with cell-essential proteins and facilitate cell attachment.

Cell Source and Culture

Articular cartilage was aseptically harvested from the femoral condyles and femoral heads of neonatal pigs. The cartilage was pooled, minced, and digested overnight in an incubator with 0.1% collagenase Type II in Dulbecco's Modified Eagle Medium (DMEM) containing 5% fetal bovine serum (FBS) and 1% antibiotic antimycotic solution (100 U/ml penicillin, 0.1 mg/ml streptomycin, 0.25 μg/ml amphotericin B). After enzymatic isolation, the cell solution was filtered through a 100μm filter to separate isolated chondrocytes from undigested material. The chondrocytes were seeded into two Corning Hyperflasks and cultured till near confluence. The chondrocytes were detached from the hyperflasks using 0.25% trypsin-EDTA.

To create the bilayered constructs, 10 million chondrocytes were seeded into a Millicell hanging transwell for 24-well plates (6.5 mm diameter, 3.0 μm PET membrane) and allowed to settle. The wells of the 24-well plate were filled with half complete medium containing 5% fetal bovine serum (FBS) and 1% antibiotic antimycotic solution (100 U/ml penicillin, 0.1 mg/ml streptomycin, 0.25 μg/ml amphotericin B) and half defined chondrogenic medium containing 1% ITS+Premix (6.25 μg/ml insulin, 6.25

μg/ml transferring, 6.25 μg/ml selenious acid, 1.25 mg/ml bovine serum albumin, 5.35 μg/ml linoleic acid), 0.1 μM dexamethasone, 50 μg/ml ascorbate-2 phosphate, 1 mM sodium pyruvate, 40 μg/ml L-proline, 1% antibiotic antimycotic solution, and 10 ng/ml of TGF-β3. Following the initial culture in half complete medium and half defined chondrogenic medium, the constructs were cultured in defined chondrogenic medium which was replaced every three or four days. After two weeks of culture, an additional 10 million chondrocytes were added to each insert, along with a chitosan scaffold. The constructs were cultured for another six weeks to allow for maturation and integration.

Porcine BMSCs were obtained as described earlier. The BMSCs were seeded into two T-175 flasks and then split into nine T-175 flasks after the flasks reached near confluence. The BMSCs were detached from the nine T-175 flasks using 0.25% trypsin-EDTA. The BMSCs were used to create bilayered constructs following the same protocol as described previously involving chondrocytes.

Scanning Electron Microscopy

The chitosan scaffolds and the scaffold-free cartilage were fixed in 2.5% glutaraldehyde, dehydrated in a graded ethanol series, and chemically dried with Hexamethyldisilazane (HMDS). Samples were mounted to stubs using carbon tape and sputter coated with gold-palladium. The samples were viewed with a JEOL JSM-6500F at 5 kV. Images of the scaffold-free cartilage's surface were acquired, along with images of the surface and pores of the chitosan scaffold.

Biphasic Constructs (15-mL Centrifuge Tube)

Cell Source and Culture

Porcine articular chondrocytes were obtained, expanded, and harvested as described earlier. Approximately 2 ml of a 2% molten agarose solution in DMEM was poured into 15 ml polypropylene centrifuge tubes and allowed to gel at 4°C. A suspension containing 5 million cells was then added to each tube and centrifuged at 1000*g* for 3 minutes to create a thin, compacted cell layer. Chitosan scaffolds, formed in transwells as described earlier, were placed into the 15 mL tubes and centrifuged at 200*g* in order to embed the scaffolds into the cell layer. Initally, the 15 mL tubes were filled with 5 mL complete medium containing 5% fetal bovine serum (FBS) and 1% antibiotic antimycotic solution (100 U/ml penicillin, 0.1 mg/ml streptomycin, 0.25 μg/ml amphotericin B) and 5 mL defined chondrogenic medium. The constructs were replenished with defined chondrogenic medium about once a week. The biphasic constructs were maintained in a standard tissue culture incubator at 37°C and 5% CO_2 for the entire study. After six weeks, constructs were fixed in 10 % neutral buffered formalin for three hours and then transferred to 70% ethanol.

Histology

The fixed constructs were sent to the University of Alabama-Birmingham's Center for Metabolic Bone Disease core laboratory for processing. The constructs were embedded in paraffin and sectioned for staining with Hemotoxyline and Eosin (H&E), Toluidine Blue, and Safranin-O.

Results

CaP Formation

Samples were examined by TEM for qualitative assessment of crystalline CaP formation. TEM micrographs of the control chitosan prepared without $CaCl_2$ and NaH_2PO_4 reveal that CaP crystals did not form on the chitosan after 24 hours in precipitation solution.

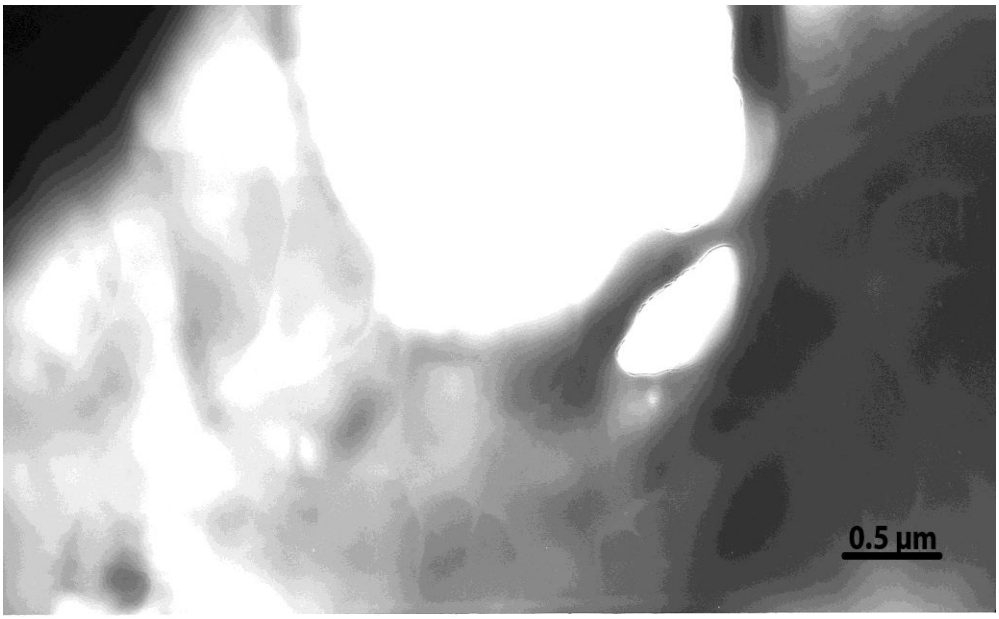

Figure 3.3 10,000X TEM micrograph of chitosan without calcium phosphate after 24 hours in precipitation solution.

TEM micrographs of the chitosan prepared with $CaCl_2$ and NaH_2PO_4 reveal CaP crystals dispersed throughout the chitosan for the 10 minute and 24 hour samples (Fig. 3.4).

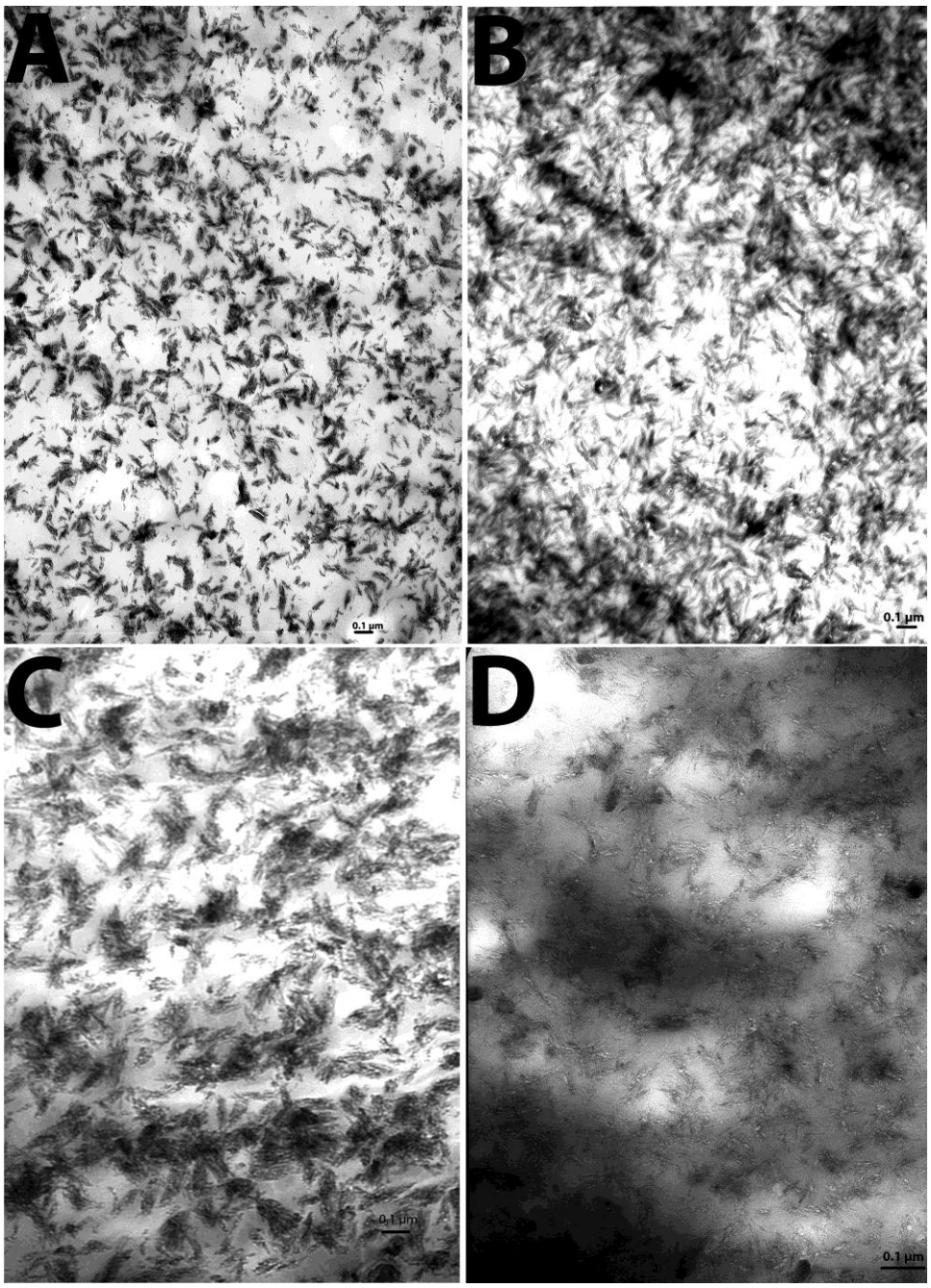

Figure 3.4 **(A)** 10,000X TEM micrograph of chitosan with calcium phosphate after 10 minutes in precipitation solution. **(B)** 10,000X TEM micrograph of chitosan with calcium phosphate after 24 hours in precipitation solution. **(C)** 50,000X TEM micrograph of chitosan with calcium phosphate after 10 minutes in precipitation solution. **(D)** 50,000X TEM micrograph of chitosan with calcium phosphate after 24 hours in precipitation solution.

BMSC Attachment to Microspheres

The BMSCs seemed to attach and encase the chitosan microspheres upon initial gross examination after 24 hours of culture**.** Samples were examined by SEM for qualitative assessment of cell attachment. Figure 3.5 shows the surface morphology of the control chitosan microsphere. The rough and textured morphology of the chitosan microsphere is presumably beneficial for cell attachment and growth due to the increased surface area. The uneven surface topology results in many depressions and cavities that could enhance the strength of the cell-chitosan interface.

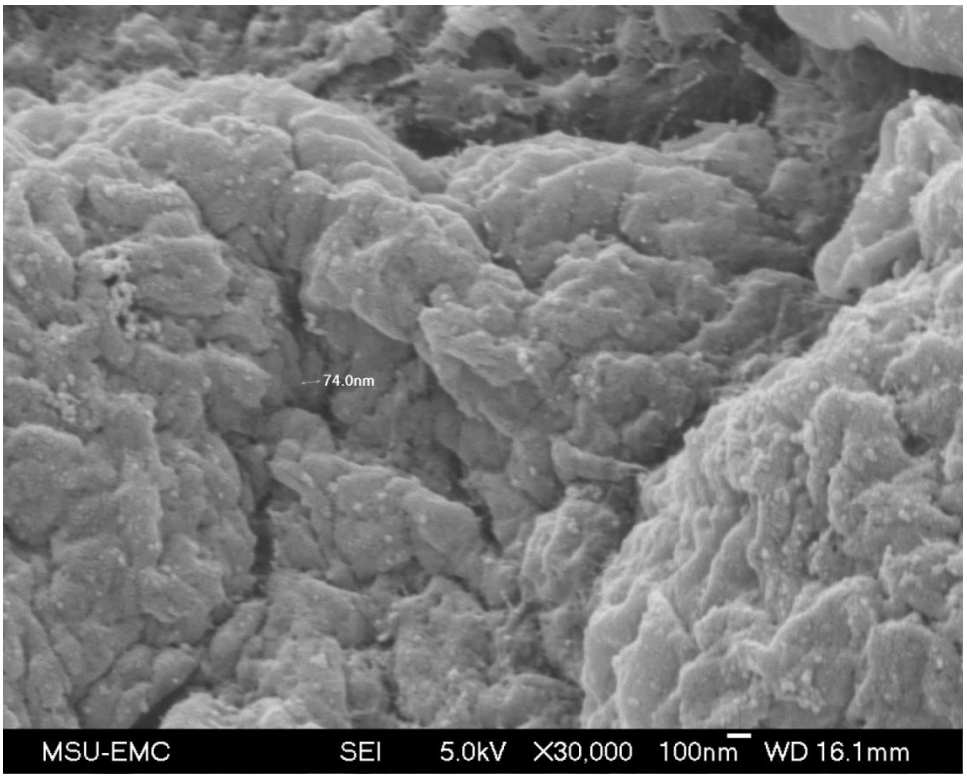

Figure 3.5 30,000X SEM micrograph of a chitosan microsphere's surface morphology.

Figure 3.6**,** an image taken at low magnification, shows the majority of a chitosan microsphere encased by cellular material. In some areas, the layer of tissue appears to contact and attach to the microsphere, whereas in other areas the tissue appears to form an encasement around the microsphere rather than directly attaching to the chitosan.

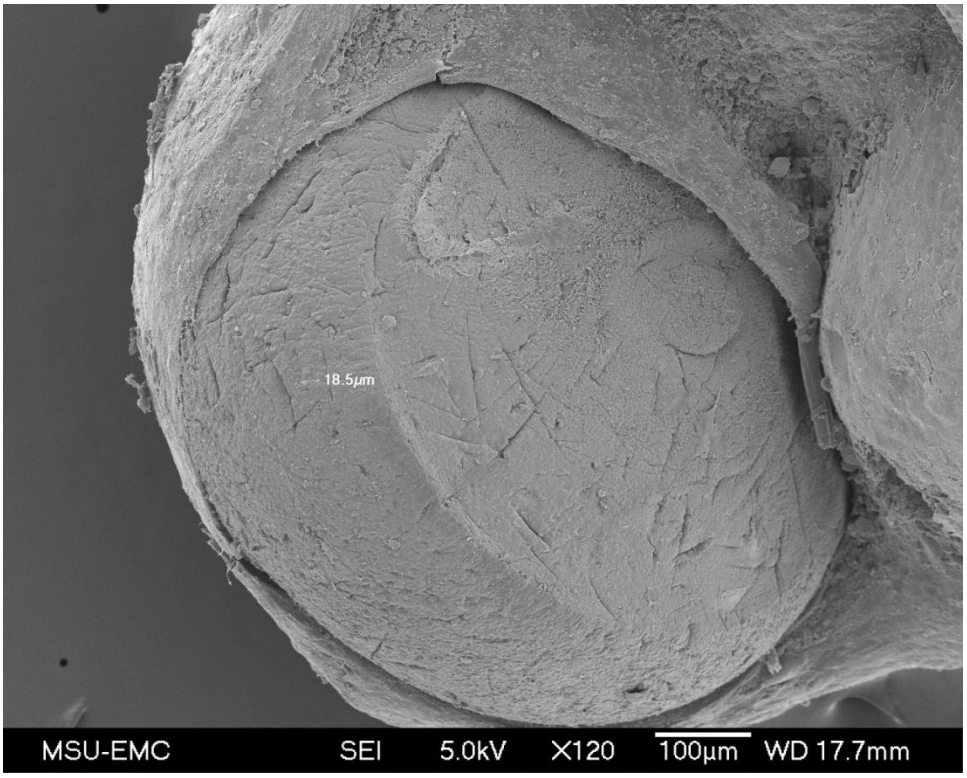

Figure 3.6 120X SEM micrograph of a chitosan microsphere encased by porcine BMSCs.

At higher magnification, the BMSCs seem to adhere to the chitosan fairly well (Fig. 3.7). Further magnification shows what seems to be a layer of extracellular material covering the surface of the chitosan microsphere (Fig. 3.8).

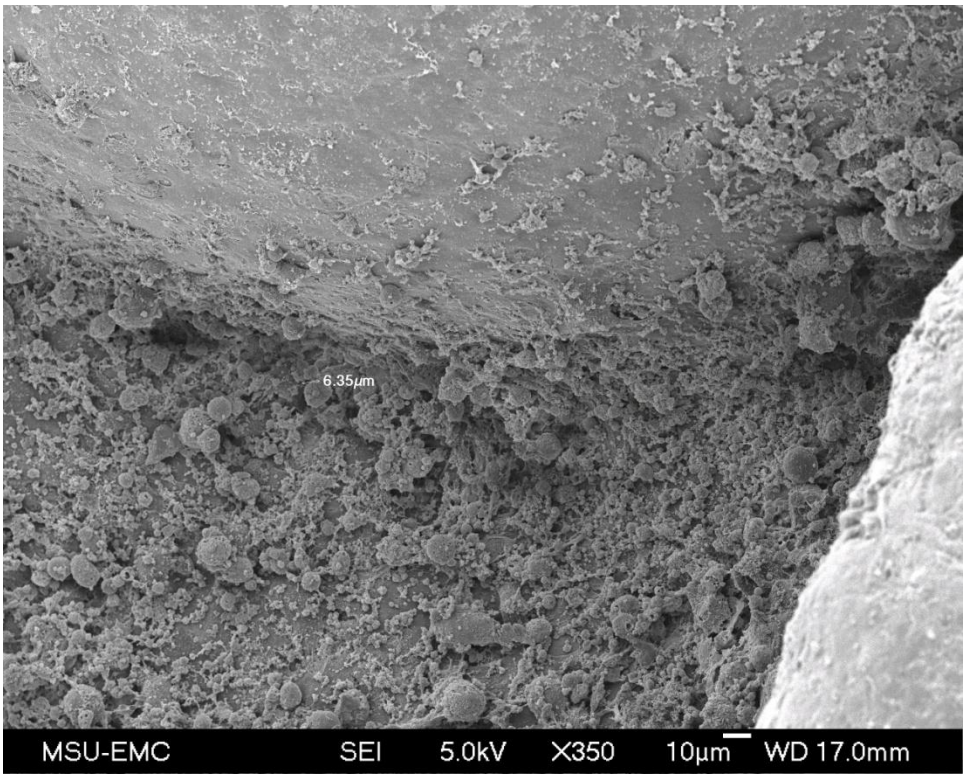

Figure 3.7 350X SEM micrograph of porcine BMSCs attached to the surface of a chitosan microsphere.

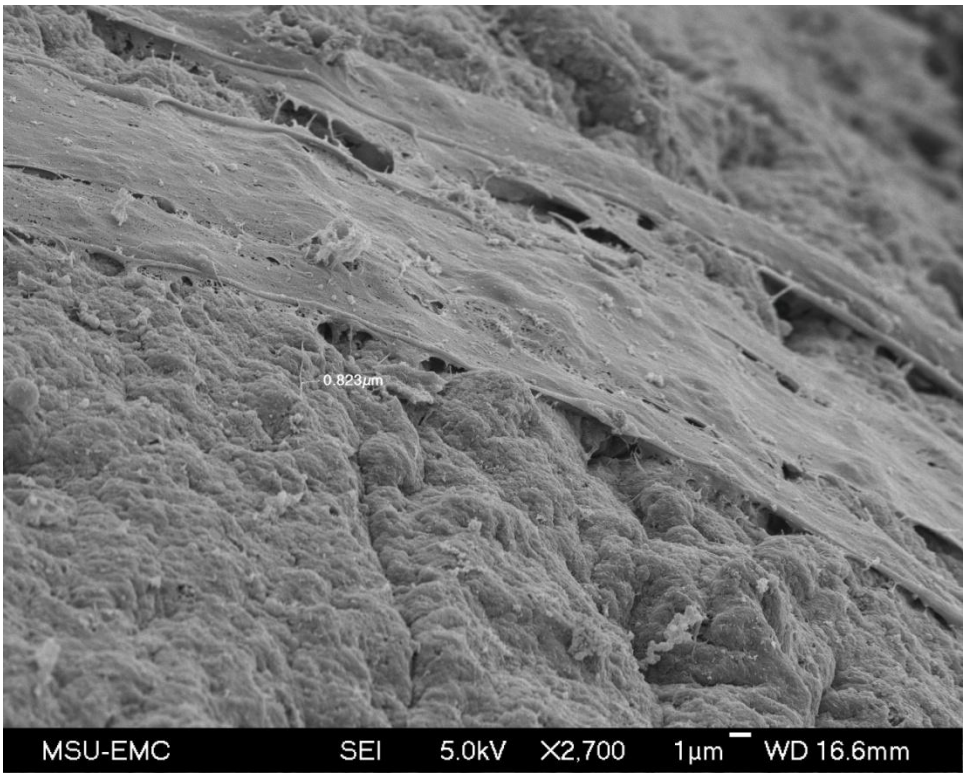

Figure 3.8 2700X SEM micrograph of ECM from porcine BMSCs covering the surface of a chitosan microsphere.

Biphasic Scaffold (Transwell)

The goal was to create a biphasic construct consisting of a layer of scaffold-free tissue engineered cartilage affixed to a scaffold comprised of fused chitosan microspheres. Gross examination revealed that the chondrocytes were able to consolidate into a layer of scaffold-free tissue engineered cartilage in the transwell; however, the layer of tissue engineered cartilage did not integrate into the chitosan scaffold. Extraction from the transwell yielded two completely separate entities with the layer of cartilage shearing off of the scaffold with relative ease.

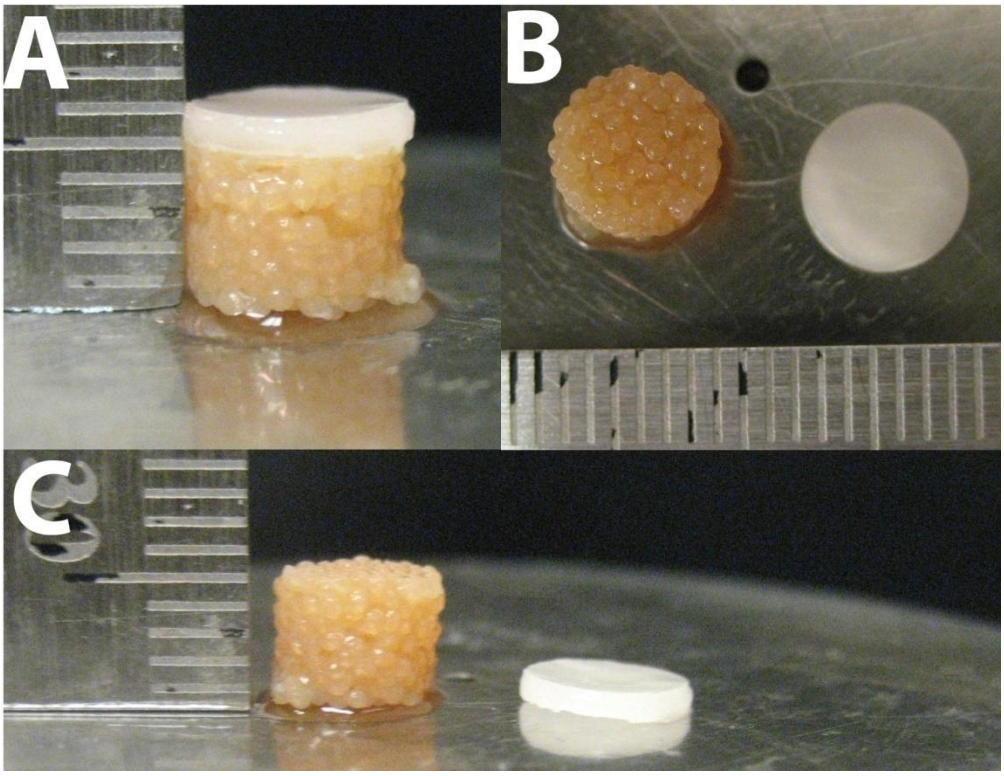

Figure 3.9 (A) Bilayered construct consisting of an upper layer of scaffold-free cartilage supported underneath by a chitosan scaffold composed of fused microspheres. (B) Top and (C) side view of the separated bilayered construct.

SEM images of scaffold-free cartilage revealed a flat, smooth surface with circular chondrocytes and large amounts of ECM (Fig. 3.10). Further magnification showed chondrocytes embedded and surrounded by a dense ECM (Fig. 3.11).

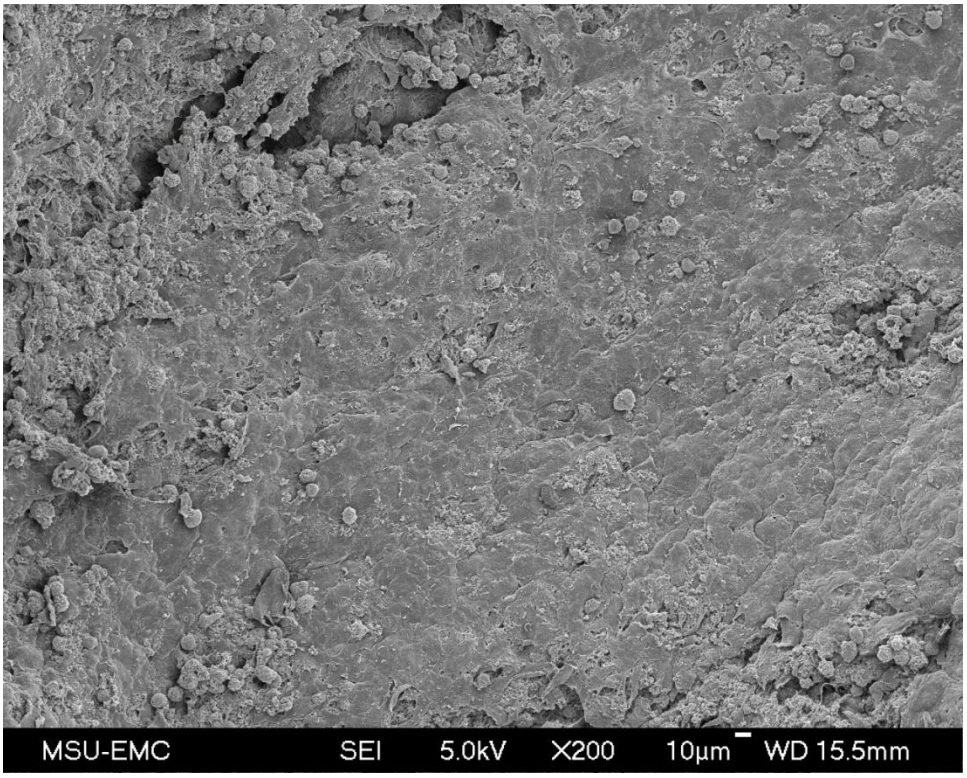

Figure 3.10 200X SEM micrograph of the surface of scaffold-free tissue engineered cartilage formed from porcine chondrocytes.

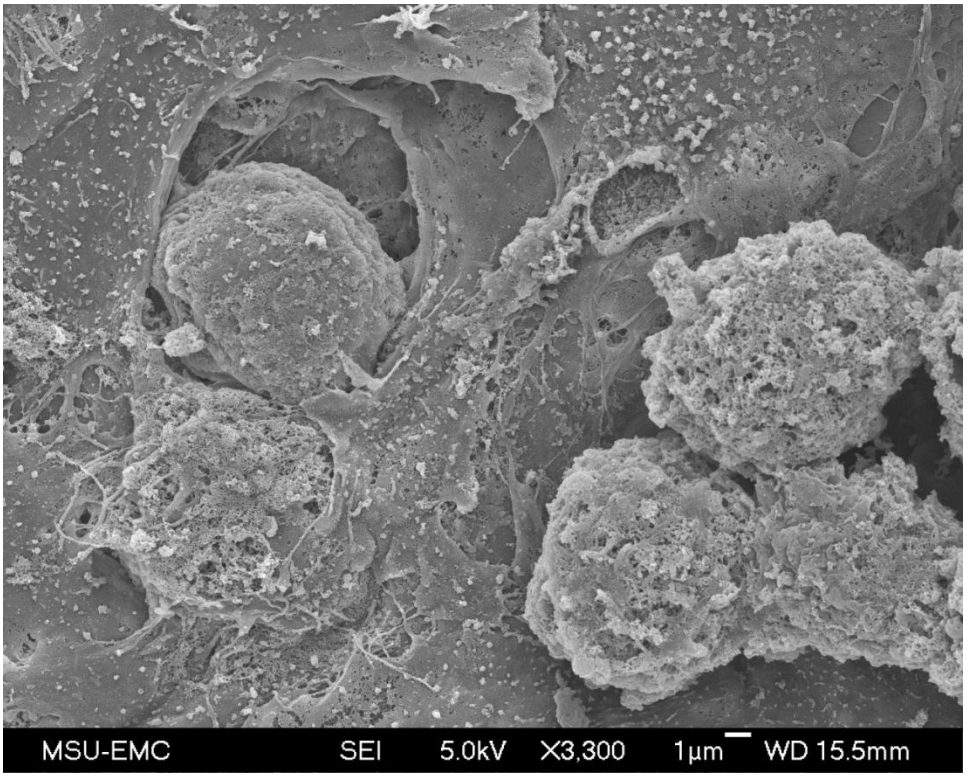

Figure 3.11 3300X SEM micrograph scaffold-free tissue engineered cartilage formed from porcine chondrocytes.

Examination of the chitosan scaffold by SEM showed chondrocytes had begun to fill the pores and bridge gaps between microspheres with ECM (Fig. 3.12) and that cells had firmly adhered to the surfaces of the microspheres and maintained a rounded morphology (Fig. 3.13).

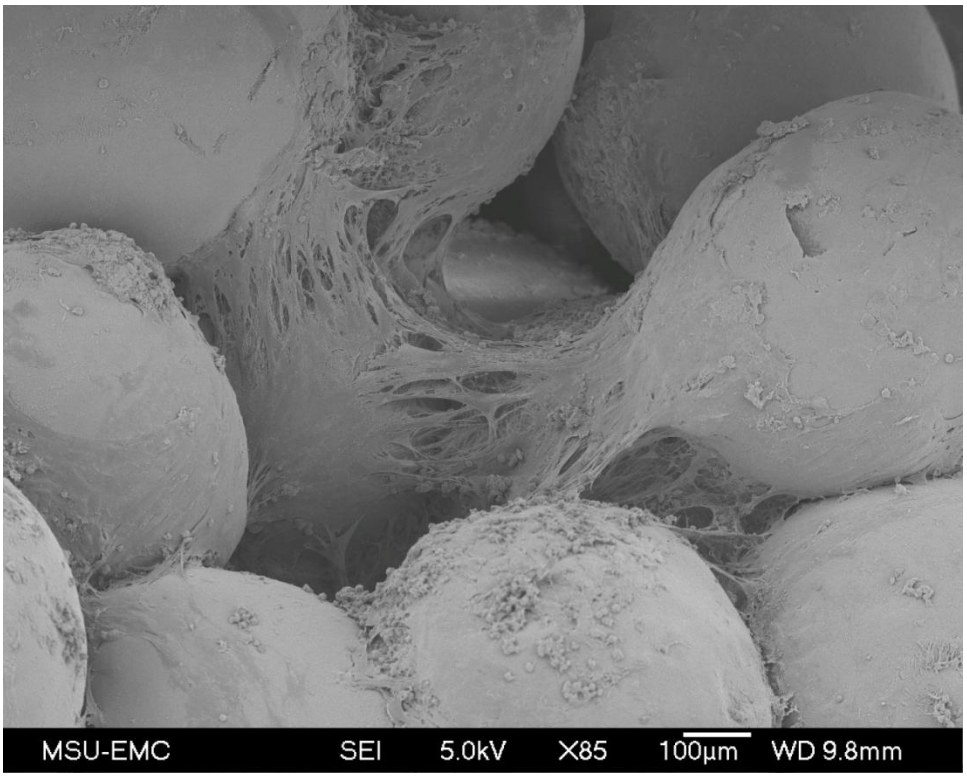

Figure 3.12 85X SEM micrograph of porcine chondrocytes attached to fused chitosan microspheres.

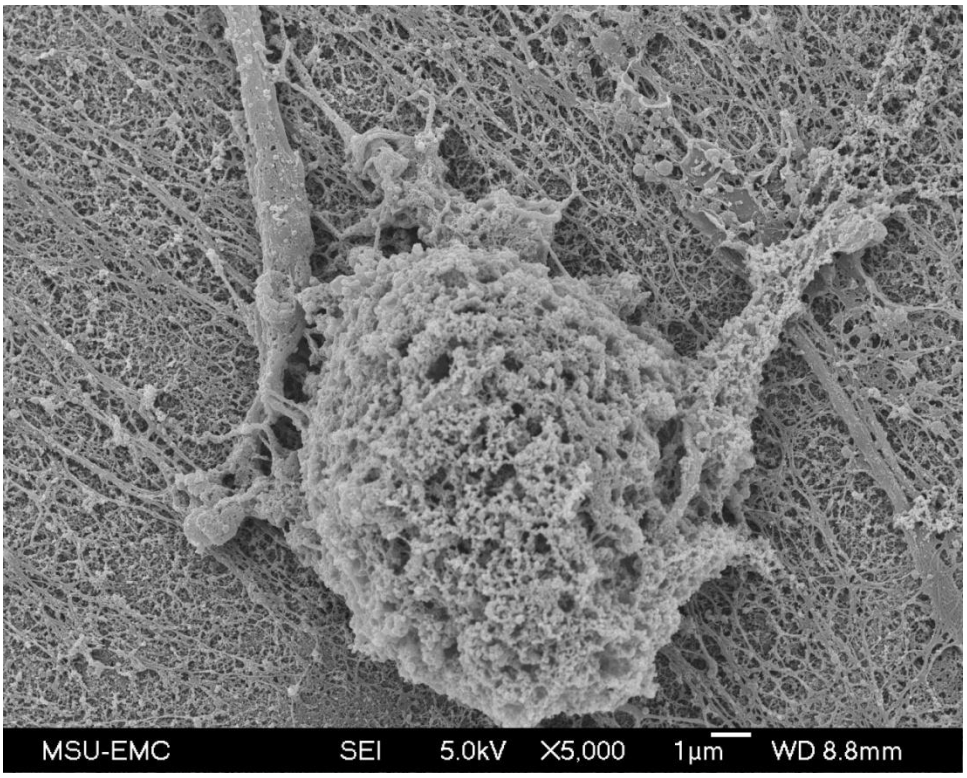

Figure 3.13 5,000X SEM micrograph of a porcine chondrocyte attached to the surface of a fused chitosan microsphere.

Examination of chitosan scaffolds seeded with BMSCs showed cells readily attached to the surface of the scaffold and beginning to fill in spaces between microspheres (Fig. 3.14). The BMSCs also had a rounded morphology characteristic of chondrogenic differentiation (Fig. 3.15).

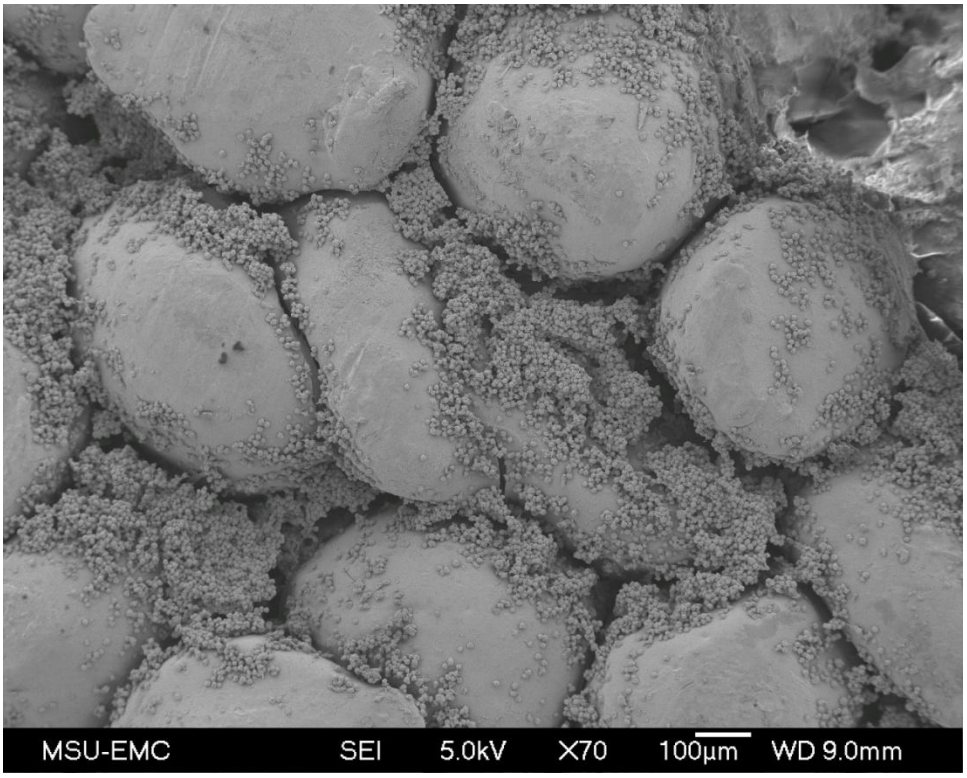

Figure 3.14 70X SEM micrograph of porcine BMSCs attached to fused chitosan microspheres.

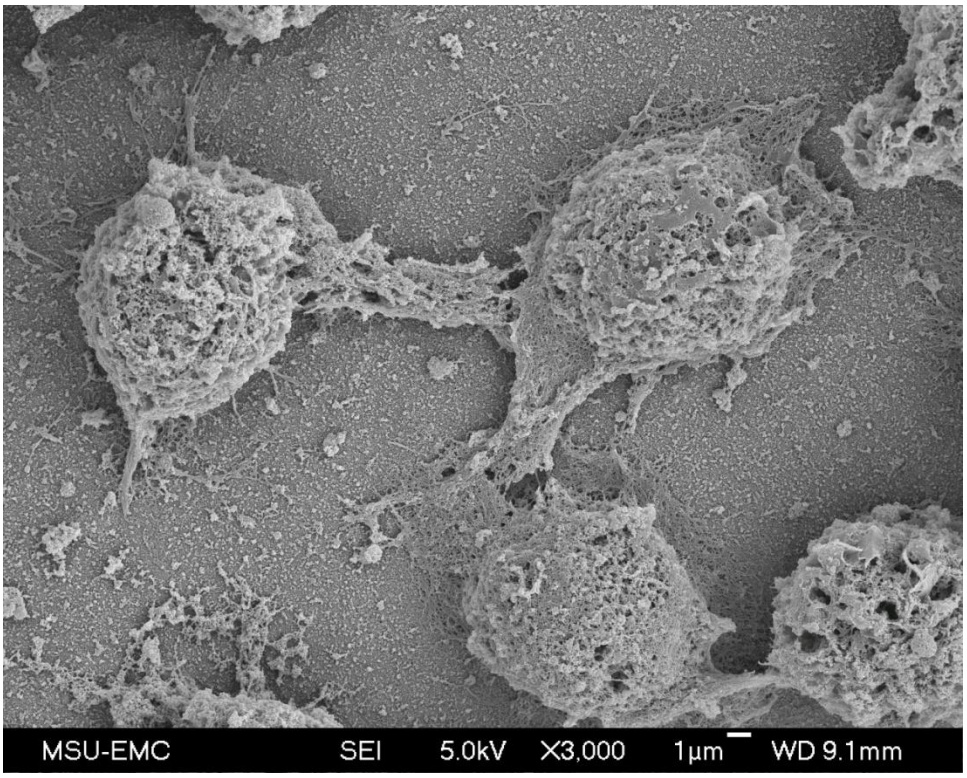

Figure 3.15 3,000X SEM micrograph of porcine BMSCs attached to the surface of a fused chitosan microsphere.

Biphasic Construct (15-mL Centrifuge Tube)

The second effort to create a biphasic construct involved centrifuging a chondrocyte cell suspension in 15 mL tubes with agarose bottoms. Removal of the construct from the 15 mL tube after six weeks of culture revealed that the layer of cartilage was not affixed to the chitosan scaffold. The cartilage adhered around the exterior forming a ring around the scaffold (Fig. 3.16). Hemotoxylin and Eosin (H&E) stained sections showed that the tissue was not only attached to the exterior of the scaffold but also infiltrated into the scaffold between the microspheres (Fig. 3.17). Figure 3.18 shows the tissue encompassing an entire microsphere. Sections were also stained with Toluidine Blue and Safranin-O for proteoglycan assessment, both of which

display intense staining which is indicative of a matrix rich in proteoglycans (Fig. 3.19, 3.20).

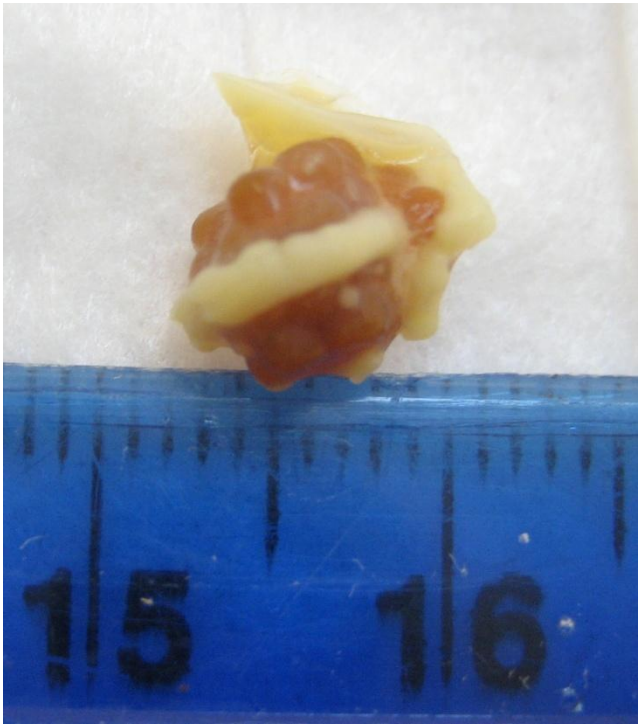

Figure 3.16 Gross appearance of a biphasic construct formed in 15-mL centrifuge tubes.

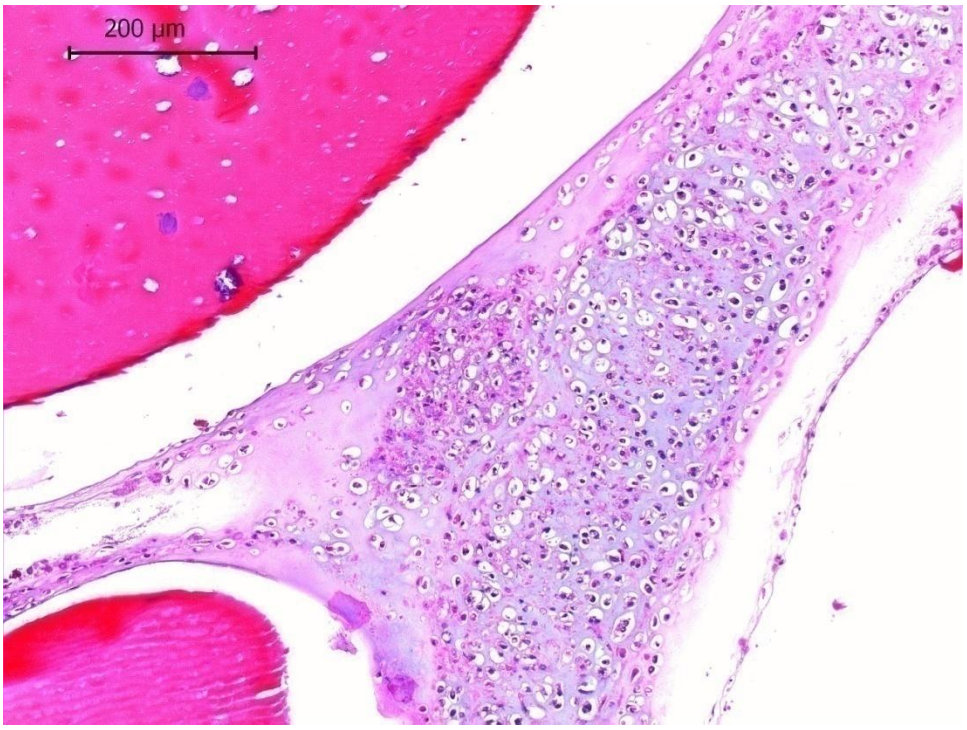

Figure 3.17 10X H&E section of a bilayered construct showing cartilage growth around and between chitosan microspheres.

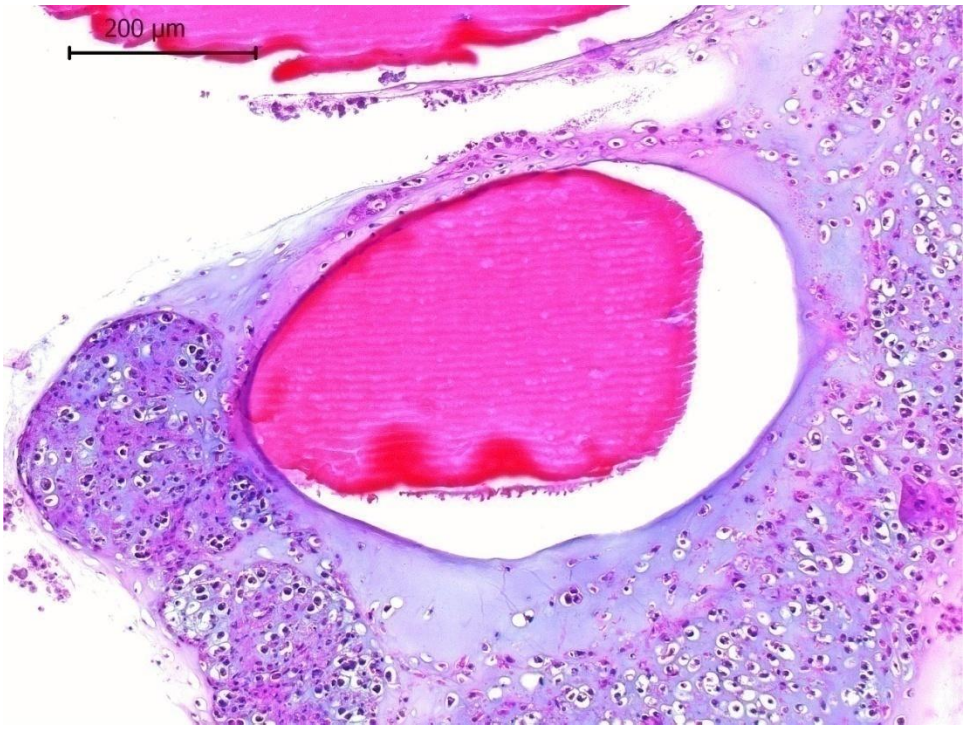

Figure 3.18 10X H&E section of a bilayered construct showing cartilage encompassing an entire chitosan microsphere.

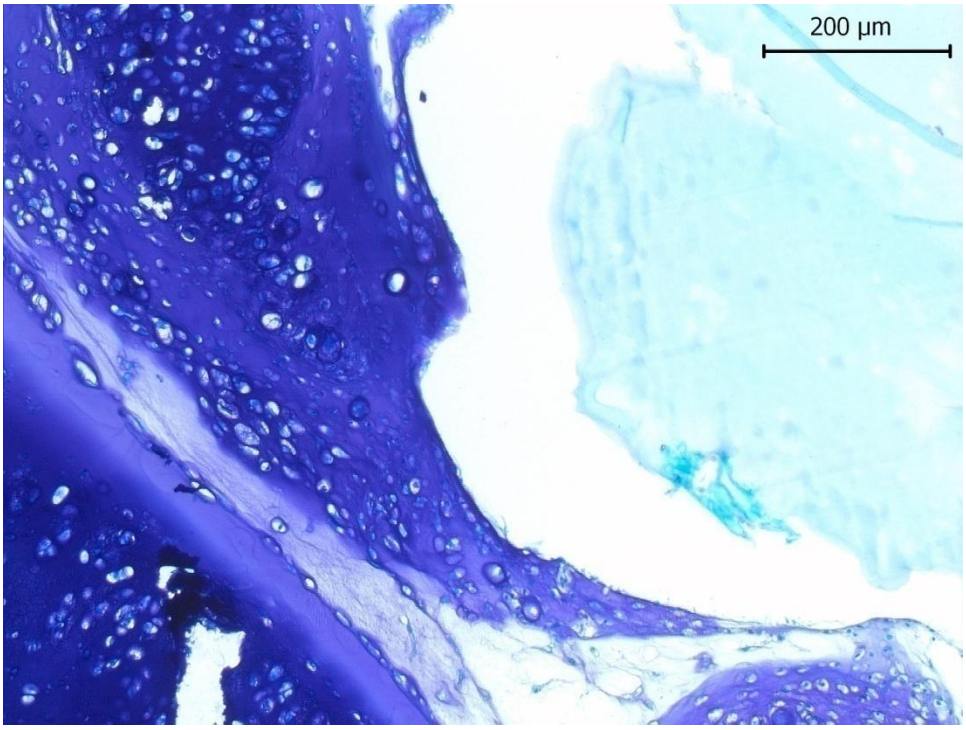

Figure 3.19 10X toluidine blue section of scaffold-free cartilage around a chitosan microsphere.

Figure 3.20 10X safranin-O section of scaffold-free cartilage cultured on a chitosan scaffold.

Discussion

Chitosan has been regarded as one of the most promising biopolymers for bone and tissue engineering. Chesnutt et al. have designed and characterized a novel chitosan/nanocrystalline calcium phosphate composite scaffold for bone regeneration. This work extends that study to investigate the potential application of chitosan in tissue engineering cartilage.

We have demonstrated the ability to form chitosan into defined geometries such as disks and various sized microspheres. Our microsphere fabrication method, which involves an air line attached to a syringe pump, allows for the formation of various sized

microspheres based on the rate of air flow. The microspheres can in turn be packed into molds of various shapes and fused with acetic acid to from three dimensional porous structures. The porosity of the three dimensional construct can be adjusted based on the size of the microspheres.

This study investigating CaP crystal formation on chitosan showed that the process occurred almost instantaneously. Qualitative assessment by SEM showed little difference between chitosan soaked in precipitation solution for 10 minutes and chitosan soaked in precipitation solution for 24 hours. Since CaP crystalline formation is not a time dependent process, the chitosan needs only to remain in the precipitation solution until it solidifies.

The initial investigation involving cell attachment to chitosan demonstrated that the chitosan was able to support the attachment of BMSCs. BMSCs not only attached to the chitosan, but also were found to produce ECM covering areas of the chitosan surface. Confirming cell attachment to chitosan microspheres was necessary in moving toward creating bilayered constructs.

For the creation of a bilayered construct, the transwells were utilized as a mold to fuse together the chitosan microspheres to create scaffolds and to confine the chondrocytes, thus resulting in a scaffold and cell layer with a circular geometry and equivalent diameters. Transwell inserts have previously been used to successfully create tissue engineered, scaffold-free cartilage with a defined geometry and smooth surface [32, 78]. Ideally, this method would yield a bilayered construct consisting of tissue engineered cartilage integrated with a porous chitosan scaffold. Unfortunately, the tissue engineered cartilage failed to integrate with the chitosan scaffold. Two cell sources,

porcine chondrocytes and porcine BMSCs, were used and neither resulted in a strong attachment between the cartilage and scaffold. Poor adhesion and integration between the cartilage layer and scaffold could be due to the second cell seeding not efficiently attaching to the previously formed cartilage as a result of poor diffusion and nutrient supply. Most likely, the reduced efficacy of the cells to integrate the cartilage layer and scaffold is a result of the cells being constrained between the layer of cartilage and the chitosan scaffold. Nutrient supply and diffusion to the cells through the transwell's PET membrane may have been prevented by the layer of cartilage and any exchange between the bulk media and media within the transwell may have been hindered by the chitosan scaffold. Failure of the cartilage layer to integrate with the scaffold may also be due to insufficient pore diameter. Small pores limit the degree to which the tissue can penetrate the scaffold. Increasing the diameter of the microspheres will lead to larger pore sizes and possibly improve tissue integration into the scaffold.

Our creation of a bilayered scaffold using 15-mL centrifuge tubes differed from the transwell method in a couple of ways. First, the chondrocytes were centrifuged to create a cell layer instead of being allowed to settle and consolidate on their own. Centrifugation of chondrocytes has been shown to increase proteoglycan synthesis [79], which could improve the attachment process between the cartilage layer and scaffold. Also, instead of merely placing the scaffold on the cell layer, the scaffold was added and then spun at 200*g* to embed the scaffold in the cell layer. Although the creation of a bilayered scaffold was unsuccessful, we were able to show tissue attachment to the chitosan scaffold as opposed to only cell attachment as seen in the past. Histological evaluations confirm that the cartilage was indeed attached to the chitosan scaffold. The

space seen between the tissue and chitosan can be attributed to histological processing and shrinkage of the chitosan.

This study extended the work of Chesnutt et al. involving novel chitosan/ nanocrystalline calcium phosphate composite scaffolds for bone regeneration to cartilage tissue engineering. Chesnutt has already shown the composite scaffolds are able to support osteoblast attachment and proliferation. Our results have demonstrated the scaffold's ability to also support chondrocyte and BMSC cell attachment, thus making the scaffold a possible candidate for producing biphasic constructs for osteochondral repair. In the future, it will be necessary to assess cell attachment quantitatively by measuring DNA or utilizing a MTS assay. Culture conditions and duration will need to be optimized in order to ensure the strong attachment of the cartilage layer to the chitosan scaffold. Much more research will be required in order to create a bilayered construct consisting of a layer of tissue engineered cartilage attached to a porous chitosan scaffold; however, we have demonstrated the potential of novel chitosan/nanocrystalline calcium phosphate composite scaffolds for osteochondral repair.

CHAPTER IV

SUMMARY

The two main goals of this dissertation were to investigate the effect of Tissue Growth Technologies' CartiGen Bioreactor on scaffold-free tissue engineered cartilage and to explore the potential use of composite chitosan/CaP scaffolds for tissue engineering biphasic scaffolds for osteochondral defects. In the first study, a novel method for producing sizable tissue engineered cartilage from neonatal porcine chondrocytes utilizing a scaffold-free approach was demonstrated. Conditioning of the cartilage in Tissue Growth Technologies' CartiGen bioreactor resulted in an enhancement of the cartilage's biochemical and biomechanical properties.

In the second study, the ability of novel chitosan/nanocrystalline calcium phosphate composite scaffolds to support the attachment of porcine chondrocytes and BMSCs and the integration of tissue engineered cartilage with a chitosan scaffold was investigated. The study demonstrated the successful attachment of both chondrocytes and BMSCs to the chitosan microspheres. Successful attachment studies warranted further attempts to produce bilayered constructs consisting of a layer of tissue engineered cartilage attached to a chitosan scaffold composed of fused microspheres. Although bilayered constructs demonstrated poor integration between the tissue layer and scaffold, the potential for these chitosan microspheres in osteochondral repair is evident.

REFERENCES

1. Schulz, R. and A. Bader, *Cartilage tissue engineering and bioreactor systems for the cultivation and stimulation of chondrocytes.* European Biophysics Journal, 2007. **36**(4): p. 539-568.

2. Buckwalter, J.A., V.C. Mow, and A. Ratcliffe, *Restoration of Injured or Degenerated Articular Cartilage.* J Am Acad Orthop Surg, 1994. **2**(4): p. 192-201.

3. Mankin, H.J., *The response of articular cartilage to mechanical injury.* J Bone Joint Surg Am, 1982. **64**(3): p. 460-466.

4. Shapiro, F., S. Koide, and M.J. Glimcher, *Cell origin and differentiation in the repair of full-thickness defects of articular cartilage.* J Bone Joint Surg Am, 1993. **75**(4): p. 532-553.

5. Felson, D.T., et al., *Osteoarthritis: New Insights. Part 1: The Disease and Its Risk Factors.* Annals of Internal Medicine, 2000. **133**(8): p. 635-646.

6. Lawrence, C.R., et al., *Estimates of the prevalence of arthritis and other rheumatic conditions in the United States: Part II.* Arthritis & Rheumatism, 2008. **58**(1): p. 26-35.

7. Clouet, J., et al., *From osteoarthritis treatments to future regenerative therapies for cartilage.* Drug Discovery Today, 2009. **14**(19-20): p. 913-925.

8. Newman, A.P., *Articular Cartilage Repair.* The American Journal of Sports Medicine, 1998. **26**(2): p. 309-324.

9. Lutzner, J., et al., *Surgical options for patients with osteoarthritis of the knee.* Nat Rev Rheumatol, 2009. **5**(6): p. 309-316.

10. Steinwachs, M.R., T. Guggi, and P.C. Kreuz, *Marrow stimulation techniques.* Injury, 2008. **39**(1, Supplement 1): p. 26-31.

11. Nehrer, S. and T.O.M. Minas, *Treatment of Articular Cartilage Defects.* Investigative Radiology, 2000. **35**(10): p. 639-646.

12. Tamer, A. and M.T. Hincke, *Strategies for Articular Cartilage Lesion Repair and Functional Restoration.* Tissue Engineering Part B: Reviews. **0**(0).

13. Miller, T.T., *Imaging of knee arthroplasty.* European Journal of Radiology, 2005. **54**(2): p. 164-177.

14. Dennis, D.A., *Evaluation of painful total knee arthroplasty.* The Journal of Arthroplasty, 2004. **19**(4, Supplement 1): p. 35-40.

15. Gill, G.S., A.B. Joshi, and D.M. Mills, *Total condylar knee arthroplasty. 16- to 21-year results*. 1999. 210-5.

16. Carranza-Bencano, A., et al., *Comparative Study of the Reconstruction of Articular Cartilage Defects with Free Costal Perichondrial Grafts and Free Tibial Periosteal Grafts: An Experimental Study on Rabbits.* Calcified Tissue International, 1999. **65**(5): p. 402-407.

17. O'Driscoll, S.W., *Articular Cartilage Regeneration Using Periosteum.* Clinical Orthopaedics and Related Research, 1999. **367**: p. S186-S203.

18. Redman, S.N., S.F. Oldfield, and C.W. Archer, *Current strategies for articular cartilage repair.* Eur Cell Mater, 2005. **9**: p. 23-32; discussion 23-32.

19. Ferruzzi, A., et al., *Autologous Chondrocyte Implantation in the Knee Joint: Open Compared with Arthroscopic Technique. Comparison at a Minimum Follow-up of Five Years.* J Bone Joint Surg Am, 2008. **90**(Supplement_4): p. 90-101.

20. Brittberg, M., et al., *Articular Cartilage Engineering with Autologous Chondrocyte Transplantation: A Review of Recent Developments.* J Bone Joint Surg Am, 2003. **85**(suppl_3): p. 109-115.

21. Iwasa, J., et al., *Clinical application of scaffolds for cartilage tissue engineering.* Knee Surgery, Sports Traumatology, Arthroscopy, 2009. **17**(6): p. 561-577.

22. Langer, R. and J.P. Vacanti, *Tissue engineering.* Science, 1993. **260**(5110): p. 920-926.

23. Chung, C. and J.A. Burdick, *Engineering cartilage tissue.* Advanced Drug Delivery Reviews, 2008. **60**(2): p. 243-262.

24. Seyedin, S.M., D.M. Rosen, and P.R. Segarini, *Modulation of Chondroblast Phenotype by Transforming Growth Factor-Beta.* Pathology and Immunopathology Research, 1988. **7**(1-2): p. 38-42.

25. Kim, S.E., et al., *Porous chitosan scaffold containing microspheres loaded with transforming growth factor-[beta]1: Implications for cartilage tissue engineering.* Journal of Controlled Release, 2003. **91**(3): p. 365-374.

26. Rosier, R.N., et al., *Transforming Growth Factor Beta: An Autocrine Regulator of Chondrocytes.* Connective Tissue Research, 1989. **20**(1): p. 295-301.

27. Hunter, W., *Of the structure and disease of articulating cartilages. 1743.* Clin Orthop Relat Res, 1995(317): p. 3-6.

28. Hu, J.C. and K.A. Athanasiou, *A Self-Assembling Process in Articular Cartilage Tissue Engineering.* Tissue Engineering, 2006. **12**(4): p. 969-979.

29. Jin, R.L., et al., *Scaffold-Free Cartilage Fabrication System Using Passaged Porcine Chondrocytes and Basic Fibroblast Growth Factor.* Tissue Engineering Part A, 2009. **15**(8): p. 1887-1895.

30. Ando, W., et al., *Cartilage repair using an in vitro generated scaffold-free tissue-engineered construct derived from porcine synovial mesenchymal stem cells.* Biomaterials, 2007. **28**(36): p. 5462-5470.

31. Katakai, D., et al., *Compressive properties of cartilage-like tissues repaired in vivo with scaffold-free, tissue engineered constructs.* Clinical Biomechanics, 2009. **24**(1): p. 110-116.

32. Elder, S.H., et al., *Production of Hyaline-like Cartilage by Bone Marrow Mesenchymal Stem Cells in a Self-Assembly Model.* Tissue Engineering Part A, 2009. **15**(10): p. 3025-3036.

33. Murdoch, D.A., et al., *Chondrogenic Differentiation of Human Bone Marrow Stem Cells in Transwell Cultures: Generation of Scaffold-Free Cartilage.* Stem Cells, 2007. **25**(11): p. 2786-2796.

34. Hayes, A.J., et al., *Macromolecular Organization and In Vitro Growth Characteristics of Scaffold-free Neocartilage Grafts.* J. Histochem. Cytochem., 2007. **55**(8): p. 853-866.

35. Naumann, A., et al., *Tissue Engineering of Autologous Cartilage Grafts in Three-Dimensional in Vitro Macroaggregate Culture System.* Tissue Engineering, 2004. **10**(11-12): p. 1695-1706.

36. Nagai, T., et al., *Optimization of Allograft Implantation Using Scaffold-Free Chondrocyte Plates.* Tissue Engineering Part A, 2008. **14**(7): p. 1225-1235.

37. Han, E., et al., *Shaped, Stratified, Scaffold-free Grafts for Articular Cartilage Defects.* Clinical Orthopaedics and Related Research®, 2008. **466**(8): p. 1912-1920.

38. Stoddart, M.J., L. Ettinger, and H.J. Häuselmann, *Generation of a scaffold free cartilage-like implant from a small amount of starting material.* Journal of Cellular and Molecular Medicine, 2006. **10**(2): p. 480-492.

39. Jubel, A., et al., *Transplantation of De Novo Scaffold-Free Cartilage Implants Into Sheep Knee Chondral Defects.* The American Journal of Sports Medicine, 2008. **36**(8): p. 1555-1564.

40. Hu, J.C. and K.A. Athanasiou, *The Effects of Intermittent Hydrostatic Pressure on Self-Assembled Articular Cartilage Constructs.* Tissue Engineering, 2006. **12**(5): p. 1337-1344.

41. Elder, B.D. and A.A. Kyriacos, *Effects of confinement on the mechanical properties of self-assembled articular cartilage constructs in the direction orthogonal to the confinement surface.* Journal of Orthopaedic Research, 2008. **26**(2): p. 238-246.

42. Bian, L., et al., *Dynamic Mechanical Loading Enhances Functional Properties of Tissue-Engineered Cartilage Using Mature Canine Chondrocytes.* Tissue Engineering Part A, 2009. **0**(0).

43. Seidel, J.O., et al., *Long-term culture of tissue engineered cartilage in a perfused chamber with mechanical stimulation.* Biorheology, 2004. **41**(3): p. 445-458.

44. Davisson, T., et al., *Static and dynamic compression modulate matrix metabolism in tissue engineered cartilage.* Journal of Orthopaedic Research, 2002. **20**(4): p. 842-848.

45. Stoddart, M.J., E. Ladina, and H. Hans Jörg, *Enhanced matrix synthesis in de novo, scaffold free cartilage-like tissue subjected to compression and shear.* Biotechnology and Bioengineering, 2006. **95**(6): p. 1043-1051.

46. Davisson, T., R.L. Sah, and A. Ratcliffe, *Perfusion Increases Cell Content and Matrix Synthesis in Chondrocyte Three-Dimensional Cultures.* Tissue Engineering, 2002. **8**(5): p. 807-816.

47. Kisiday, J.D., et al., *Effects of dynamic compressive loading on chondrocyte biosynthesis in self-assembling peptide scaffolds.* Journal of Biomechanics, 2004. **37**(5): p. 595-604.

48. Mow, V.C., et al., *Biphasic Creep and Stress Relaxation of Articular Cartilage in Compression: Theory and Experiments.* Journal of Biomechanical Engineering, 1980. **102**(1): p. 73-84.

49. Soltz, M.A. and G.A. Ateshian, *Experimental verification and theoretical prediction of cartilage interstitial fluid pressurization at an impermeable contact interface in confined compression.* Journal of Biomechanics, 1998. **31**(10): p. 927-934.

50. Waldman, S., et al., *Characterization of cartilagenous tissue formed on calcium polyphosphate substrates <I>in vitro</I>.* Journal of Biomedical Materials Research, 2002. **62**(3): p. 323-330.

51. Vunjak-Novakovic, G., et al., *Bioreactor cultivation conditions modulate the composition and mechanical properties of tissue-engineered cartilage.* Journal of Orthopaedic Research, 1999. **17**(1): p. 130-138.

52. Martin, I., et al., *Modulation of the mechanical properties of tissue engineered cartilage.* Biorheology, 2000. **37**(1): p. 141-147.

53. Riesle, J., et al., *Collagen in tissue-engineered cartilage: Types, structure, and crosslinks.* Journal of Cellular Biochemistry, 1998. **71**(3): p. 313-327.

54. Julkunen, P., et al., *Biomechanical, biochemical and structural correlations in immature and mature rabbit articular cartilage.* Osteoarthritis and Cartilage, 2009. **17**(12): p. 1628-1638.

55. Mow, V., Ratclif A., *Structure and function of articular cartilage and meniscus.* Basic Orthopaedic Biomechanics, 1997: p. p. 113-78.

56. Sah, R., B.T. Stephen, and J.G. Alan, *Differential effects of serum, insulin-like growth factor-I, and fibroblast growth factor-2 on the maintenance of cartilage physical properties during long-term culture.* Journal of Orthopaedic Research, 1996. **14**(1): p. 44-52.

57. Mauck, R.L., et al., *Influence of Seeding Density and Dynamic Deformational Loading on the Developing Structure/Function Relationships of Chondrocyte-Seeded Agarose Hydrogels.* Annals of Biomedical Engineering, 2002. **30**(8): p. 1046-1056.

58. Sah, R., et al., *Biosynthetic response of cartilage explants to dynamic compression.* Journal of Orthopaedic Research, 1989. **7**(5): p. 619-636.

59. Chowdhury, T.T., et al., *Temporal regulation of chondrocyte metabolism in agarose constructs subjected to dynamic compression.* Archives of Biochemistry and Biophysics, 2003. **417**(1): p. 105-111.

60. Lima, E.G., et al. *The Effect of Applied Compressive Loading on Tissue-Engineered Cartilage Constructs Cultured with TGF-ÃƒÂŸ3*. in *Engineering in Medicine and Biology Society, 2006. EMBS '06. 28th Annual International Conference of the IEEE*. 2006.

61. LeBaron, R.G. and K.A. Athanasiou, *Ex vivo synthesis of articular cartilage.* Biomaterials, 2000. **21**(24): p. 2575-2587.

62. Khan, A., et al., *The effect of continuous culture on the growth and structure of tissue-engineered cartilage.* Biotechnology Progress, 2009. **25**(2): p. 508-515.

63. Darling, E.M. and K.A. Athanasiou, *Articular Cartilage Bioreactors and Bioprocesses.* Tissue Engineering, 2003. **9**(1): p. 9-26.

64. Lee, C.R., A.J. Grodzinsky, and M. Spector, *Biosynthetic response of passaged chondrocytes in a type II collagen scaffold to mechanical compression.* Journal of Biomedical Materials Research, 2003. **64A**(3): p. 560-569.

65. Okamoto, Y., et al., *Evaluation of chitin and chitosan on open would healing in dogs.* J Vet Med Sci, 1995. **57**(5): p. 851-4.

66. No, H.K., et al., *Antibacterial activity of chitosans and chitosan oligomers with different molecular weights.* International Journal of Food Microbiology, 2002. **74**(1-2): p. 65-72.

67. Hu, Q., et al., *Preparation and characterization of biodegradable chitosan/hydroxyapatite nanocomposite rods via in situ hybridization: a potential material as internal fixation of bone fracture.* Biomaterials, 2004. **25**(5): p. 779-785.

68. Madihally, S.V. and H.W.T. Matthew, *Porous chitosan scaffolds for tissue engineering.* Biomaterials, 1999. **20**(12): p. 1133-1142.

69. Uchida, A., et al., *The use of calcium hydroxyapatite ceramic in bone tumour surgery.* J Bone Joint Surg Br, 1990. **72-B**(2): p. 298-302.

70. Cooke, F.W., *Ceramics in Orthopedic Surgery.* Clinical Orthopaedics and Related Research, 1992. **276**: p. 135-146.

71. Wang, M., D. Porter, and W. Bonefield, *Processing, characterization, and evaluation of hydroxyapatite-reinforced polyethylene composites.* British Ceramics and Transactions Journal, 1994. **93**: p. 91.

72. Zhang, R. and X.M. Peter, *Poly(alpha-hydroxyl acids)/hydroxyapatite porous composites for bone-tissue engineering. I. Preparation and morphology.* Journal of Biomedical Materials Research, 1999. **44**(4): p. 446-455.

73. Zhang, Y. and Z. Miqin, *Synthesis and characterization of macroporous chitosan/calcium phosphate composite scaffolds for tissue engineering.* Journal of Biomedical Materials Research, 2001. **55**(3): p. 304-312.

74. Varma, H.K., et al., *Porous calcium phosphate coating over phosphorylated chitosan film by a biomimetic method.* Biomaterials, 1999. **20**(9): p. 879-884.

75. Kong, L., et al., *Preparation and characterization of nano-hydroxyapatite/chitosan composite scaffolds.* Journal of Biomedical Materials Research Part A, 2005. **75A**(2): p. 275-282.

76. Yamaguchi, I., et al., *Preparation and microstructure analysis of chitosan/hydroxyapatite nanocomposites.* Journal of Biomedical Materials Research, 2001. **55**(1): p. 20-27.

77. Chesnutt, B., et al., *Design and characterization of a novel chitosan/nanocrystalline calcium phosphate composite scaffold for bone regeneration.* Journal of Biomedical Materials Research Part A, 2009. **88A**(2): p. 491-502.

78. Murdoch, A., et al., *Chondrogenic Differentiation of Human Bone Marrow Stem Cells in Transwell Cultures: Generation of Scaffold-Free Cartilage.* Stem Cells, 2007. **25**(11): p. 2786-2796.

79. Inoue, H., et al., *Stimulation of Proteoglycan and DNA Syntheses in Chondrocytes by Centrifugation.* Journal of Dental Research, 1990. **69**(9): p. 1560-1563.

APPENDIX A

PROTOCOL

Fetal Pig BMSC Isolation

Materials
Autoclave beakers, Pyrex dish, PBS, drape
Syringe
50 ml tubes
10% bleach
70% ethanol
Method
Remove femurs or tibias using aseptic technique
Remove all connective tissue from bones
Keep bones on ice
Rinse briefly in 10% bleach
Wash in 70% ethanol
Allow to dry in Pyrex dish on ice
Break bones in half using sterile wire cutters and place in syringe, broken side down
Place syringe in 50 ml tube and centrifuge at 200*g* for 10 minutes
Remove syringes and pool marrow for seeding into flasks

SEM Fixation

Samples fixed in 2.5% Glutaraldehyde	1-2 hrs
Dehydrated in series of ethanol:	
70%	1 hr
80%	1 hr
90%	1 hr
100%	1 hr
100%	overnight
50% EtOH – 50% HMDS	4-6 hrs
100% HMDS	overnight

Remove HMDS and allow to air dry. Store with desiccant until sputter coating.

Papain Digestion

Prepare immediately before use:

Add 1 mg cysteine per mL of 50 mM Sodium Acetate (pH to 6 with acetic acid) [weigh cysteine first]
Add 10 µl papain per mL of Sodium Acetate/cysteine
Warm water bath to 37 ℃
Digest scaffold in 1 ml at 60 ℃ overnight

Blyscan Sulfated Glycosaminoglycan Assay

Set up assay:
Label a set of 1.5 ml microcentrifuge tubes. If sufficient material is available, run duplicate samples.

Prepare:
[1] Reagent blanks, (100 µl of distilled water
or the test sample buffer).

[2] Glycosaminoglycan standards,
(aliquots containing 1.0, 2.0, 3.0, 4.0 & 5.0 µg).

[3] Test samples, (volumes: 10 to 100 µl).
Adjust the contents of all tubes to 100 µl with
distilled water or appropriate buffer.

To each tube add 1 ml Blyscan dye reagent and cap all of the tubes.

Mixing:
Place tubes on a mechanical shaker for 30 minutes, (or manually shake at 5 minute intervals). During this time period the Blyscan dye will bind to sulfated glycosaminoglycans. The dye reagent is designed so that the sGAG-dye complex will precipitate out of solution.

Centrifuging:
Transfer the tubes to a micro centrifuge and spin the tubes at > 10,000 x g for 10 minutes. It is important to firmly pack the insoluble pellet of the sGAG-dye complex at the bottom of the tubes, so as to avoid any loss during draining.

Draining:
The unbound dye solution is removed by carefully inverting and draining the tubes. Any remaining droplets can be removed from the tubes by *gently* tapping the inverted tube on a paper tissue. Do not attempt to physically remove any fluid that is in close contact to the deposit.

Release of bound dye:
To each tube add 1 ml of the dissociation reagent. Re-cap the tubes and release the bound dye into solution. A vortex mixer is suitable. When the bound dye has been dissolved, usually within 10 minutes, the samples are ready for measurement. The color is light stable, but should be read within 2 hours. Keep the tubes capped until ready for measurement.

Measurement:
Multiwell plate reader, set to read at 450 nm. Transfer 200 µl aliquots of samples from tubes to the wells of a 96 well, multiwell plate. Measure absorbance of reagent blanks glycosaminoglycan standards and the test samples. Subtract the reagent blank reading from the standard and test sample readings.

Sircol Collagen Assay

Set Up Assay:
Label a set of 1.5ml microcentrifuge tubes. If sufficient test material is available run duplicate samples.

Prepare:
Reagent blanks - 100µl of deionised water or 0.5M acetic
acid or fresh cell culture medium or extraction buffer.

Collagen standards - use aliquots containing 5, 10, 25, and 50 µg of the Collagen Reference Standard. Make each standard up to 100µl using the same solvent as the reagent blanks.

Test samples - use volumes between 10 and 100µl. Adjust the contents of all tubes to 100 µl with distilled water or appropriate buffer.

To each tube add 1 mL sircol Dye reagent and cap all of the tubes; mix contents by inverting.

Mixing:
Place tubes in a gentle mechanical shaker for 30 minutes, (or manually mix at 5 minute intervals). During this time period a collagen-dye complex will form and precipitate out from the soluble unbound dye.

Centrifuging:
Transfer the tubes to a microcentrifuge and spin at >10,000 r.p.m. for 10 minutes. It is important to firmly pack the insoluble pellet of the collagen-dye complex at the bottom of the tubes, as to avoid any pellet loss during draining of unbound dye.

Draining:
The unbound dye solution is removed by carefully inverting and draining the tubes. Any remaining droplets can be removed from the tubes by *gently* tapping the inverted tube on a paper tissue. Do not attempt to physically remove any fluid that is in close contact to the deposit.

Release of bound dye:
To each tube add 1 mL of the Alkali reagent. Recap tubes and release the collagen bound dye into solution. A vortex mixer is suitable. When all of the bound dye has been dissolved, usually within 10 minutes, the samples are ready for measurement. The color is light stable, but should be read within 2 to 3 hours. Keep tubes capped until ready for measurement.

Measurement:
Multiwell plate reader, set to read at 540 nm. Transfer 200 µl aliquots of samples from tubes to the wells of a 96 well, multiwell plate. Measure absorbance of reagent blanks, collagen standards and the test samples. Subtract the reagent blank reading from the standard and test sample readings.